THE EFFECTS OF IRRADIATION WITH PROTONS ON THE
ELECTRICAL PROPERTIES AND DEFECT CONFIGURATIONS OF THE
COMPOUND Bi_2Te_3

by

PRAVEEN CHAUDHARI

B. Tech. (Hons.), Indian Institute of Technology
Kharagpur, 1961

S.M., Massachusetts Institute of Technology
Cambridge, Massachusetts, 1963

Submitted in partial fulfillment of the requirements
for the degree of
DOCTOR OF SCIENCE

at the
Massachusetts Institute of Technology
1965

Signature of Author
Department of Metallurgy

_____

Signature of Professor
in Charge of Research

_____

Signature of Chairman of
Departmental Committee on
Graduate Students

_____

ABSTRACT

THE EFFECTS OF IRRADIATION WITH PROTONS ON THE

ELECTRICAL PROPERTIES AND DEFECT CONFIGURATIONS OF THE

COMPOUND Bi_2Te_3

by

PRAVEEN CHAUDHARI

Submitted to the Department of Metallurgy in December 1965 in partial fulfillment of the requirements for the degree of Doctor of Science.

Single crystals of p-type Bi_2Te_3 were irradiated at room temperature with 7.5 Mev protons. The Hall coefficient and resistivity were measured as functions of temperature from $82^{\circ}K$ to room temperature after successive irradiations. The change in the magneto-resistance coefficient on irradiation was measured at $82^{\circ}K$. Foils of the compound Bi_2Te_3 were irradiated at two levels of flux and examined by transmission electron microscopy.

The Hall coefficient of irradiated specimens measured at $82^{\circ}K$ increased exponentially with increasing integrated dose. A dose of 1.2×10^{16} protons per cm^2 converted the specimen from p-type to n-type. The net effect of irradiation was to introduce donors, which were fully ionized at $82^{\circ}K$. The value of the Fermi level decreased with increasing irradiation dosage.

The resistivity of the specimens increased with irradiation. The exponent of the temperature coefficient of the resistivity decreased and became negative after irradiation with a dose of 1.2×10^{16} protons per cm^2. If it is assumed that the major mechanisms of scattering of charge carriers are ionized imperfection and lattice scattering, satisfactory agreement between the experimental and calculated values of the resistivity was obtained. The number of defects calculated from the values of Hall coefficient and resistivity was more than an order of magnitude smaller than the value calculated from theories of radiation damage. This difference was attributed in part to annealing out of defects during irradiation.

The magneto-resistance coefficient measured at $82^{\circ}K$ decreased with increasing irradiation and appeared to reach saturation after a dose of 1.0×10^{16} protons per cm^2. The band structure parameters calculated from the measured values of the Hall coefficient, resistivity, and magneto-resistance changed rapidly after doses of 1.0×10^{16} protons per cm^2.

After irradiation at a flux of 1.8×10^{13} protons per cm^2 per sec to an integrated dose of 5.5×10^{18} protons per cm^2, point defect clusters were observed. Some of the clusters could be shown to be aligned along the $\langle 10\bar{1}0 \rangle$ and $\langle 11\bar{2}0 \rangle$ directions. After irradiation at a flux of 3.0×10^{13} protons per cm^2 per sec to an integrated dose of 5.5×10^{18} protons per cm^2, clusters of interstitial atoms and clusters of vacancies were observed.

Pits having hexagonal cross sections with sides parallel to $\langle 11\bar{2}0 \rangle$ directions were present in irradiated specimens. They are believed to have formed by evaporation from the surface at the elevated temperatures generated by the proton current and to have been nucleated by defects introduced by the irradiation. The pits were observed to grow in the electron microscope, presumably because of further evaporation due to the heating of the specimen by the electron beam.

Thesis Supervisor: Michael B. Bever

Title: Professor of Metallurgy

TABLE OF CONTENTS

LIST OF TABLES

LIST OF FIGURES

ACKNOWLEDGEMENTS

The author wishes to thank his thesis supervisor, Professor Michael B. Bever, for many stimulating discussions, constant advice and encouragement throughout the course of this thesis.

During this investigation the author had access to equipment and facilities in the Departments of Metallurgy and Electrical Engineering, and the Cyclotron Laboratory. For this the author would like to thank the following:

Department of Metallurgy

Professor John F. Breedis for many helpful discussions regarding the operation of the electron microscope and the interpretation of the electron micrographs;

Mr. Robert Goss for excellent instruction in the use and handling of the electron microscope;

Mr. Timothy Curran for help with the electron microscope;

Mr. Leonard Sudenfield for helping with the processing of some of the electron micrographs;

Mrs. Theresa R. Walsh for typing the working draft of this thesis.

Department of Electrical Engineering

Professor Arthur C. Smith for granting the use of his equipment and also for the very valuable discussions and suggestions;

Mr. William Brennan for help with the operation of the equipment.

Cyclotron Laboratory

I. INTRODUCTION

Extensive experimental and theoretical work has been carried out on radiation damage in semiconducting elements, but little published information is available on radiation damage in semiconducting compounds.[1] Research on radiation damage in semiconducting compounds is of fundamental interest because of the mechanisms involved. At the same time such research holds practical interest because semiconducting compounds may find applications under conditions in which they are exposed to radiation.

Among the semiconducting materials, the compound Bi_2Te_3 is especially important because of its good thermoelectric properties.[2] On account of these properties this compound may find application in devices used in space vehicles. Such vehicles travel in environments where radiations, particularly protons and electrons, are present.[3] The effect of these radiations on the compound Bi_2Te_3 may therefore be of critical importance for this application. In the work reported here, irradiation with protons rather than electrons was investigated because the former may predominate in such regions as the van Allen belt.[3] Also, for comparable radiation energies and dosages, protons are likely to have greater effects on the properties of a material.[1]

In this investigation single crystals of p-type Bi_2Te_3 were irradiated with protons of 7.5 Mev energy. The Hall coefficient, resistivity, and magneto-resistance of the irradiated specimen were measured. Crystalline imperfections generated by irradiation were also examined in foils by transmission electron microscopy.

II.   REVIEW OF LITERATURE

1.   Crystal Structure of Bismuth Telluride

The compound Bi_2Te_3 has a rhombohedral crystal structure and a space group symmetry $R\bar{3}m$.[4,5]   The atoms are located at the following positions:

One atom of tellurium at   0 0 0

Two atoms of tellurium at $x_1x_1x_1$, $\bar{x}_1\bar{x}_1\bar{x}_1$ where x_1 = 0.792

Two atoms of bismuth at $x_2x_2x_2$, $\bar{x}_2\bar{x}_2\bar{x}_2$ where x_2 = 0.399

The measured lattice constants are:

a = 10.473 A.U.

α = 24° 9' 32"

To facilitate visualisation one may transform the rhombohedral into a hexagonal structure.   After this transformation, the lengths of the a-and c-axis are

a = 4.3835 A.U.

c = 30.487 A.U.

The arrangement of the atoms in the [0001] direction of the hexagonal system consists of a series of layers of tellurium and bismuth atoms. The sequence of layers is as follows:

$-Te^{(1)}-Bi-Te^{(2)}-Bi-Te^{(1)}-Te^{(1)}-Bi-Te^{(2)}-Bi-Te^{(1)}-Te^{(1)}-Bi-Te^{(2)}-Bi-Te^{(1)}-$

These fifteen layers account for the length of the c-axis in the hexagonal system. It should be noted that the layers repeat themselves after every fifth layer as far as their chemical composition is concerned. The layers of atoms are stacked in the [0001] direction in the stacking order of face centered cubic crystals.

2. Bonding

The accepted bonding scheme for the compound Bi_2Te_3 is van der Waals bonding between the atoms of the $Te^{(1)}$-$Te^{(1)}$ layers, covalent and ionic bonding between the atoms of the $Te^{(1)}$ and Bi layers, and covalent bonding resulting from a sp^3d^2 hybridization between the atoms of the two Bi layers and the $Te^{(2)}$ layer.[6] As a result of the weak van der Waals bonding between the atoms of the $Te^{(1)}$-$Te^{(1)}$ layers, these layers are the cleavage planes in the compound Bi_2Te_3. They also are the planes on which the dislocations lie.[7]

3. Band Structure

On the basis of the measurements of the Hall coefficient, resistivity, and magneto-resistance, the band structure of the compound Bi_2Te_3 is proposed to be many valleyed;[8] the energy extrema of the valleys are on the reflection planes in reciprocal space. The width of the energy gap has been determined, and the reported values range from 0.16 to 0.21 ev.[9,10]

4.   Defect Structure

Single crystals of the compound Bi_2Te_3 grown from the melt of
stoichiometric composition act as p-type semiconductors.   The phase
diagram of the system bismuth-tellurium was determined in the vicinity
of the compound Bi_2Te_3.[10]   This determination was made by measurements
of the Hall coefficient and involved the assumption that at liquid
nitrogen temperature an excess bismuth or tellurium atom behaves as a
singly ionized acceptor or donor, respectively.   There is some
disagreement in the literature on the defect structures of the compound
when excess bismuth or tellurium is present.   It has been suggested that
the excess bismuth atoms occupy additional bismuth sites, with the creation
of vacancies on tellurium sites.[11]   According to an alternative
proposal antistructure defects are present.[12,13] In the case of excess
bismuth 3/5 of the excess bismuth atoms and in the case of excess
tellurium 2/5 of the excess tellurium atoms occupy tellurium or bismuth
sites, respectively.   Measurements of the density combined with the
measurements of the Hall coefficient appear to indicate that the lattice
defects are predominantly of the antistructure type, at least on the
bismuth-rich side of the stoichiometric composition.[13]

The Hall coefficient of single crystals of p-type Bi_2Te_3 quenched
from $773^{\circ}K$ was lower than of   slowly cooled single crystals; the
resistivity differed in the opposite direction.[14,15]   If the defects
introduced by quenching are assumed to be predominantly vacancies, then
the overall effect of bismuth and tellurium vacancies in p-type Bi_2Te_3

is to introduce acceptors. After sintering at various temperatures for 16 hours, compacted powders of p-type Bi_2Te_3 changed sign to an n-type carrier at temperatures of approximately $470^{\circ}K$, and reverted back to p-type after sintering at higher temperatures.[16] The investigators attributed this change of sign of the majority carrier to the formation of excess vacancies. If the excess of the two types of vacancies over the thermal equilibrium value can be assumed to be the same in the quenching and sintering experiments, then one of the two interpretations would be in error. However, the concentrations of the two types of vacancies are likely to be different in the two cases.

In another investigation the compound Bi_2Te_3 was extruded at $548^{\circ}K$ and its annealing behavior investigated.[17] After extrusion the sign of the charge carrier changed from p-type to n-type. From annealing data, the investigators concluded that the donor was a tellurium vacancy, and that its activation energy for migration was between 0.7 and 1.1 ev.

Investigation of radiation damage by γ-rays,[18,19] electrons,[20] thermal and fast neutrons[21,22,23] have been carried out on p- and n-type Bi_2Te_3. After exposure of n-type Bi_2Te_3 to irradiation from a Co^{60} source at room temperature, the thermoelectric power decreased and the resistivity increased with irradiation; they reached saturation after a dose of 6×10^6 roentgens. The effects of irradiation annealed out at room temperature within three hours. If the irradiation was carried out at the temperature of a mixture of dry ice and acetone, the thermo-electric power and the resistivity increased. The increment of the

thermoelectric power annealed out at 230°K with a half-life of 29 hours.
A specimen of p-type Bi_2Te_3 irradiated with γ-radiation from a Co^{60} source
at the temperature of a mixture of dry ice and acetone also showed an
increase in thermoelectric power.

In another investigation with γ-radiation from a Co^{60} source an
electronic effect and lattice damage were observed.[19] The electronic
effect was associated with a reduction of the Hall coefficient and
resistivity in n-type Bi_2Te_3, but with an increase in their value in p-type
Bi_2Te_3. The electronic effect annealed out within 24 hours at room
temperature. In this investigation the lattice damage reduced the Hall
coefficient and the resistivity in p-type Bi_2Te_3 and raised them in n-type.
An analysis of the annealing data led to the conclusion[19] that aggregates
of interstitial atoms are found on the basal planes, and that these
dissociate with an activation energy of 0.7 ev and that their dissociation
increases the Hall coefficient and resistivity in p-type Bi_2Te_3. From
annealing data obtained at higher temperatures, a defect identified as a
tellurium vacancy was observed to anneal out with an activation energy
of 0.9 ev. From this observation it was concluded that a tellurium
vacancy must be an acceptor. This conclusion contradicts the conclusion
reached by other investigators,[17] who annealed specimens of extruded
p-type Bi_2Te_3.

Irradiation with electrons of 2 Mev energy from a Van der Graaff
accelerator was carried out on n-type Bi_2Te_3.[20] The thermoelectric power
decreased during irradiation, but recovered subsequently. However, the

heat generated by the bombarding electrons caused oxidation and melting of the specimen, so that the effects of the defect structure due to radiation damage could not be observed.

Reactor irradiation[21,22,23] with fast neutrons of energy greater than 1 Mev and integrated dose of 10^{19} neutrons per cm^2 was carried out on shielded and unshielded specimens of n- and p-type Bi_2Te_3 maintained at 333 $\pm$ 20°K. The Seebeck coefficient on n-type specimens increased, while a p-type specimen was converted to an n-type carrier after irradiation.

5. Investigation of Defect Configuration by Transmission Electron Microscopy

Investigations of the compound Bi_2Te_3 by electron microscopy have been reported in the literature. Dislocations and dislocation networks were observed on the basal planes of this compound.[7] The Burgers vector of the dislocations was determined to be in the $\langle 2\bar{1}\bar{1}0 \rangle$ direction. Dislocation loops were observed in quasi-binary alloys of Bi_2Te_3 and Sb_2Te_3. These loops were found to lie on the basal planes of the alloys.[24,25] They were attributed to deviations from stoichiometry, which caused either an excess of antimony atoms to form interstitial loops or to an insufficient number of tellurium atoms to form vacancy loops. Such loops were observed in binary alloys of up to 60 pct Bi_2Te_3-40 pct Sb_2Te_3, but not in the range between this composition and pure Bi_2Te_3. Presumably the defects due to deviation from stoichiometry in the compound Bi_2Te_3 do not coalesce to form dislocation loops of the type observed in Sb_2Te_3 and Bi_2Te_3 alloys.

Irradiated foils of the compound Bi_2Te_3 do not appear to have been

examined in the electron microscope. Graphite, which has a similar layer structure, however, has been irradiated with neutrons and investigated by transmission electron microscopy.[26,27] Some of the defect structures in irradiated graphite were found to be vacancy aggregates and clusters of interstitials.[26] Large interstitial loops lying on the basal planes were also found in irradiated graphite.[27]

In the compound Bi_2Te_3, the nature of the defect structure is expected to be more complicated than in graphite because of the presence of two types of atom species. However, the general defect structure is not expected to be basically different. For example, in neutron irradiated MgO prismatic loops were found to lie in the (110) planes.[28]

III.   OUTLINE OF WORK

The research reported here consists of two parts.   The first part deals with an investigation of the changes in the electrical properties caused by proton irradiation and the second part with an investigation by transmission electron microscopy of the defect configuration introduced by the irradiation.

1.   Electrical Measurements

Specimens of the compound Bi_2Te_3 were irradiated in the internal beam chamber of a cyclotron.   The incident irradiation was parallel to the c-axis of the compound Bi_2Te_3.   During irradiation the target holder was water cooled, and the proton beam current was adjusted so as not to exceed a temperature rise of $75^{\circ}C$.   After irradiation the specimen was kept at liquid nitrogen temperature for seven days to allow the induced radioactivity to decay.   After this the specimen was warmed to room temperature.   After 48 hours at room temperature the electrical measurements were started.

The Hall coefficient and electrical resistivity were measured as functions of the temperature from the temperature of liquid nitrogen to room temperature.   The magneto-resistance coefficient was measured at the temperature of liquid nitrogen.   After completion of these measurements the specimen was cooled to liquid nitrogen temperature until the next irradiation run.

The Hall coefficient was measured with the magnetic field parallel

to the c-axis of Bi_2Te_3. The electric field was perpendicular to the magnetic field. The resistivity and magneto-resistance were measured along the basal planes. The tensors corresponding to the electrical resistivity, Hall coefficient, and magneto-resistance are represented as ρ_{11}, ρ_{123}, and ρ_{1133} This representation is similar to that adopted by Drabble.[8]

2. Transmission Electron Microscopy

Thin foils of Bi_2Te_3 suitable for transmission electron microscopy were placed between gold grids and irradiated. On completion of the irradiation the specimen was kept at the temperature of liquid nitrogen for seven days. After this period the specimens were examined in a Siemens Elmiskopp I and Hitachi HU-11 microscopes. The latter microscope which was equipped with a low temperature stage was used for examining specimens at the temperature of liquid nitrogen.

IV. EXPERIMENTAL PROCEDURE

i. Single Crystals

Single crystals of p-type Bi_2Te_3 were prepared by Dr. J.H. Dennis
under the supervision of Prof. R.B. Adler of the Department of Electrical
Engineering. The details of the experimental procedure for preparing
the crystals has been described elsewhere.[29]   Briefly, the method
consisted of growing single crystals from a bath made up of weighed
amounts of bismuth and tellurium maintained under an atmosphere of helium.
The bismuth and tellurium were of semiconductor grade quality (99.999+pct)
and were supplied by the American Smelting and Refining Company, South
Plainfield, New Jersey.

2. Specimens for Electrical Measurements

2.1 Specimen Preparation

Single crystals of Bi_2Te_3 were cleaved with Scotch tape to remove a
layer of material about one millimeter thick from one of the surfaces
of the as-grown crystals. These crystals were cleaved again to obtain
the desired specimen which adhered to the Scotch tape. The thickness
of the specimen varied between $1.5-3.0 \times 10^{-3}$ cm. The specimen adhering
to the Scotch tape was cut to the shape and dimensions shown in Figure 1(a).
The length of the specimen at this stage of preparation exceeded the final
length (shown by dashed lines in Figure 1(a). The excess length of the
material was used to measure the final thickness of the specimen after
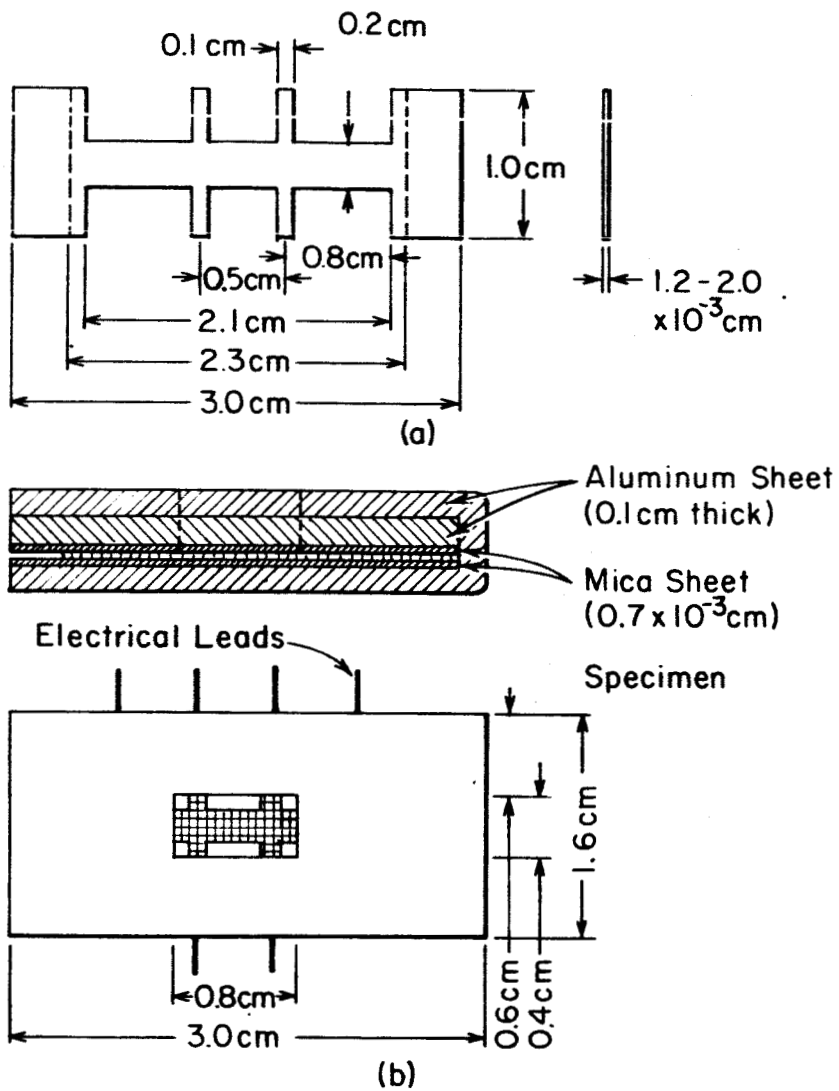
Fig. 1(a) Shape and dimensions of specimens for
electrical measurements.

(b) Holder for specimen for electrical measurements.

12

the various stages of preparation described below.

After the specimen was cut to the desired dimensions, the Scotch
tape was removed by dissolving the adhesive in toluene. Although
acetone can dissolve the adhesive faster than toluene, the Scotch tape
curled in this solvent, and this caused the specimen to bend. In
toluene the process of dissolution occured in approximately 48 hours.
At the end of this time, the specimen and Scotch tape usually separated.
The specimen was washed in acetone and ether.

The specimen, along with extra pieces of Bi_2Te_3, was placed in a Vycor
tube, which was either evacuated or filled with argon. The sealed
tube containing the specimen was heated in a muffle furnace at $350^{o}C$ for
24 hours. The purpose of the extra pieces of Bi_2Te_3 was to minimize
the extent of any reaction of the specimen with oxygen, during the heat
treatment of the specimen. After the heat treatment, the specimen was
lightly etched with a solution consisting of 1 part concentrated HNO_3,
2 parts concentrated HCl, and 2 parts H_2O. In order to reduce the rate
of etching, the etchant was kept at $0^{o}C$.

The excess length of the specimen, mentioned earlier, was now removed
with a blade. The thickness of these extra pieces was measured with a
micrometer. The ends of the specimen to which electrical leads were
to be soldered were nickel plated. The following plating solution was
used:

Nickel sulphate	$NiSo_4$. $7 H_2O$	112 gms/liter of H_2O
Nickel chloride	$NiCl_2$. $6 H_2O$	14 " " " "
Boric acid	H_3BO_3	14 " " " "

The operating current density was about 0.4 amp per cm^2. The plating bath was maintained at $50^{o}C$.

Plating was necessary because it was difficult to solder electrical leads to the unplated specimen directly as most solders do not wet the compound Bi_2Te_3. Nickel plating produces electrical leads of low contact resistance. A high contact resistance would have caused local temperature rise and this coupled with the high thermoelectric power of the compound Bi_2Te_3 would have produced extraneous voltages.

After nickel plating, the electrical leads which were made of silver wire 0.01 cm. in diameter, were soldered with a solder consisting of 60 pct lead and 40 pct tin.

2.2 Specimen Thickness

The thickness of the specimen used for the electrical measurements was chosen after consideration of the following factors: (1) the range of 7.5 Mev protons, (2) the mean free path of the protons, (3) the heat transfer by the specimen, (4) the mechanical strength of the specimen and (5) surface effects.

2.2.1 Range of 7.5 Mev protons -
If the thickness of the specimen is greater than the range of the incident protons, the protons which are retained effect the properties of the specimen. In order to avoid such effects the thickness of the specimen used must be less than the range of the incident protons.

If it is assumed that as a proton traverses a specimen of the compound Bi_2Te_3 it loses energy mainly through ionization and excitation, the range of a 7.5 Mev proton is estimated to be between 0.036 and 0.100 cm.

The details of the calculation are given in Appendix I.

2.2.2 Mean Free Path of the Protons - If the minimum energy required to displace an atom from its lattice position is E_d, the probability that the incident proton transfers energy greater than or equal to the displacement energy E_d, is related to a displacement cross-section σ_d. The number of displacement collisions made by a proton of energy E per unit length of its path is $N_0\sigma_d$, where N_0 is the number of atoms per unit volume.[1] The reciprocal of the quantity $N_0\sigma_d$ is defined as the mean free path between displacement collisions. As σ_d depends on the energy E of the proton the value of E must be known at every instant during the motion of the proton through the specimen. Since this is not possible, the specimen thickness was chosen such that each proton would undergo only one displacement collision during its passage through the specimen. On the assumption of a single collision the number of lattice defects created by the incident proton can be calculated more simply than in the case of repeated collisions.

For a 7.5 Mev proton interacting with an atom of the specimen, the displacement cross-section can be obtained by considering the interaction potential to be coulombic and neglecting the screening of the nucleus by the electron cloud.[1,30] If these assumptions are made, the displacement cross-section σ_d is given by[1]

$$\sigma_d = \int_{E_d}^{E_{p(max)}} k(E, E_p)dE_p = \frac{\pi b^2}{4} \frac{E_{p(max)}}{E_d} \tag{1}$$

In equation (1), $k(E, E_p)$ is the specific cross-section or cross-section per unit energy, E_p is the energy transferred to the struck atom, $E_p(max)$ is the the maximum energy transferred in an elastic collision if energy and momentum are conserved, and b is the classical distance of closest approach given by

$$b = \frac{2 Z_1 Z_2 e^2}{\mu v^2} \tag{2}$$

In equation (2), Z_1 and Z_2 are the atomic numbers of the incident particle and the target atom respectively, e is the electronic charge, v is the velocity of the particle relative to the atom, and μ is the reduced mass equal to $(\frac{mM}{m + M})$, where m is the mass of the target atom and M is the mass of the incident particle.

As shown by equation (1), σ_d depends on the energy of the incident particle, and since this energy decreases continuously as the particle passes through the specimen, the displacement cross-section increases. For the compound Bi_2Te_3, and an incident radiation of 7.5 Mev protons, the following two equations can be written for the displacement cross-sections $\sigma_{d,Te}(t)$, $\sigma_{d,Bi}(t)$ for a tellurium and bismuth atom respectively as a function of the depth of penetration t

$$\sigma_{d, Te}(t) = \frac{1.345 \times 10^{-18}}{E(t) E_{d,Te}} \tag{3}$$

$$\sigma_{d, Bi}(t) = \frac{2.106 \times 10^{-18}}{E(t) E_{d,Bi}} \tag{4}$$

where E(t) is the energy of the proton expressed in Mev at a depth t, and $E_{d,Te}$ and $E_{d,Bi}$ are the displacement energies in ev of tellurium and bismuth atoms respectively.

Before a displacement cross-section can be evaluated, the displacement energy must be known. This has not been determined for Bi_2Te_3 either experimentally or theoretically. However, as the bonding scheme in Bi_2Te_3 is known, a rough estimate of the displacement cross-section can be made. The model of the bonding scheme[6] shows covalent bonding between the atoms of $Te^{(1)}$ and Bi, and covalent bonding between the atoms of $Te^{(2)}$ and Bi. If the bond strength is assumed to be the same between the atoms of $Te^{(1)}$ and Bi, and $Te^{(2)}$ and Bi, then the displacement energies for the Bi and $Te^{(2)}$ are the same, and that for $Te^{(1)}$ is half that of the other two. The latter relation arises from the fact that an atom of $Te^{(1)}$ has three whereas an atom of $Te^{(2)}$ has six bonds with neighbouring atoms of bismuth.

In germanium and silicon, which have covalent bonding and relatively open structures, the displacement energy is 13 ev.[31] The displacement energy for a Bi and $Te^{(2)}$ atoms can therefore be assumed to be about 15 ev, and that for $Te^{(1)}$ about 7.5 ev. For a particle energy of 7.5 Mev, the displacement cross-sections are then given by

$$\sigma_{d,\ Te}^{(1)} = 2.4 \times 10^{-20} \ cm^2 \tag{5}$$

$$\sigma_{d,\ Te}^{(2)} = 1.2 \times 10^{-20} \ cm^2 \tag{6}$$

$$\sigma_{d,\ Bi} = 1.9 \times 10^{-20} \ cm^2 \tag{7}$$

The mean displacement cross-section per atom is 2.0×10^{-20} cm^2, so that for 3.0×10^{22} atoms per cm^3 in Bi_2Te_3 the mean free path ℓ is

$$\ell = 1.67 \times 10^{-3} \text{ cm} \tag{8}$$

The thickness of the specimen should therefore be less than 1.67×10^{-3} cm. The thickness of the specimens used in this investigation ranged from 1.2 to 1.5×10^{-3} cm.

2.2.3. <u>Heat Transfer</u> - Most of the energy lost as the particle traverses the specimen is converted into heat, so that the specimen must be cooled during irradiation. This is usually carried out by placing the specimen on a water cooled target holder. A good heat transfer path between the specimen and the target holder is essential. Alternatively, the rate of heat generated in the specimen must be decreased. For a given radiation of a certain energy a reduction of the heat generated is possible only by decreasing the thickness of the specimen. Heat transfer therefore favors thinnest possible specimens.

2.2.4. <u>Mechanical Strength</u> - The compound Bi_2Te_3 has low mechanical strength and thin specimens are fragile and difficult to handle. These specimens must therefore be mounted, which adds to the heat transfer path.

2.2.5. <u>Surface Effects</u> - A very thin specimen may no longer represent the properties of the bulk material. In particular the surface states in semiconductors may affect the electrical properties of the material. Fortunately, this effect is not important in Bi_2Te_3 because of the high density of carriers and the saturated bonds on the surface of the specimen.

2.3 Specimen Holder

Because of the difficulty in handling them, the specimens were mounted on holders which were designed so that both the irradiation and the electrical measurements could be carried out without the need for removing the specimens from the holders.

A specimen holder is shown in Figure 1(b). It was made of aluminum sheet about 0.1 cm thick. The other dimensions of the sheet were 6 cm x 1.6 cm. On one side of the sheet a window was cut out, which had the purpose of exposing a selected area of the specimen to the irradiation. The dimensions of the window were 0.8 cm x 0.4 cm. The area of the specimen to which the silver wire was soldered was not exposed to irradiation. A second piece of aluminum sheet 3 cm long, 1.6 cm wide and 0.1 cm thick with a window of the same size as the window in the first sheet was placed on the first sheet so that the two windows over-lapped. This increased the thickness of the aluminum that was exposed to the radiation so that protons could not reach the specimen except through the window.

A mica sheet 3 cm long, 1.6 cm wide and 7×10^{-4} cm thick was cleaved from a larger sheet. The cleaved sheet was joined to the aluminum sheet with rubber cement diluted with acetone. In order to obtain a firm joint with a minimum of cement, the mica sheet was pressed down firmly against the aluminum sheet and baked at 50°C for 24 hours.

The specimen was placed on the mica sheet. The electrical leads of the specimen from the edge of the solder to the end of the specimen

holder were joined to the mica sheet by Epoxy cement.   It was necessary

to do this as a slight pull on the leads tended to break the specimen.

In order to obtain good thermal contact, the specimen was cemented

to the mica sheet by placing a few drops of a dilute solution of

Duco cement in acetone near the edge of the specimen and allowing

capillary action to pull the solution between the specimen and the

mica sheet and then pressing on the specimen until the cement hardened.

The large sheet was folded along the center line so that the

window exposed the desired area of the specimen to the irradiation.

After folding, the edges of the holder were joined to each other to make

a strong compact specimen holder.   After the Epoxy had set the specimen

holder containing the specimen was placed in a pyrex tube, evacuated

and heated at $75^{o}C$ for 8 hours.   The purpose of this heat treatment was

to remove or to stabilize any structural effects in the specimen and

specimen holder that might have been introduced during preparation.

3.   Measurement of the Electrical Properties

The equipment used for measuring the electrical properties had been

built under the supervision of Prof. A.C. Smith of the Department of

Electrical Engineering.   The components of the equipment and their

calibration can be described as follows:

3.1 Magnetic Field

The magnetic field was obtained from a Varian magnet (4 in. pole

piece diameter) with a variable power supply.   The magnet was calibrated

against the current supplied to the current coils with a moving coil

gaussmeter.   A maximum field strength of 6,000 ± 100 gauss was used.

3.2 Cryostat

The cryostat shown in Figure 2 was a double walled copper chamber. The space between the walls was evacuated.   The specimen was mounted on a copper block with a large thermal capacity.   Liquid nitrogen was poured into the inner chamber to cool the copper block to 78°K. After a set of measurements had been completed at the temperature of liquid nitrogen, the nitrogen was boiled off, and the copper block allowed to warm up gradually.   Measurements were made at various temperatures between 82°K and room temperature during this period which lasted for approximately eight hours.   The temperature of the specimen was measured with a copper-constantan thermocouple.

In order to estimate the error in the measurements made during continuous heating, isothermal measurements were made by using liquid oxygen, a mixture of carbon dioxide and acetone, and a mixture of ice and water.   At the temperatures obtained in this manner, the differences between the isothermal and continuous heating measurements was less than five percent.

3.3 Circuit Diagram for the Measurement of Electrical Properties

The diagram of the circuit used in this investigation is shown in Figure 3.   A switch for reversing the polarity was required to connect a lead storage battery, with an open circuit potential of six volts to the main circuit.   A decade resistance box was placed in series with the specimen to vary the resistance between 500 and 3000 ohms. The value of the resistance was selected in relation to the resistance of the

Walls of Copper Dewar

Copper Block

Radiation Shield

Magnet

Specimen Holder

To Vacuum Pump
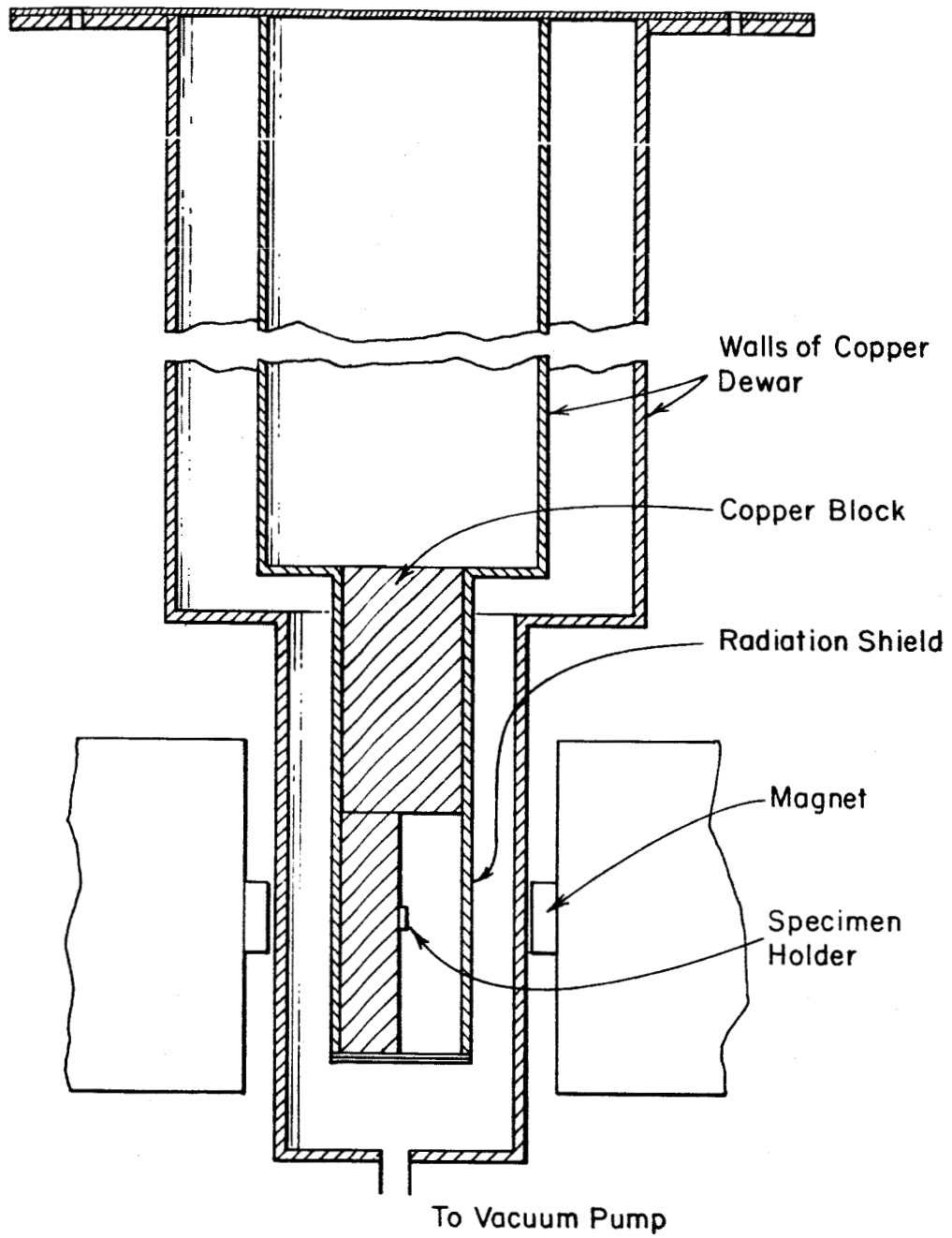
Fig. 2   Schematic arrangement of the cryostat for electrical
measurements.

22
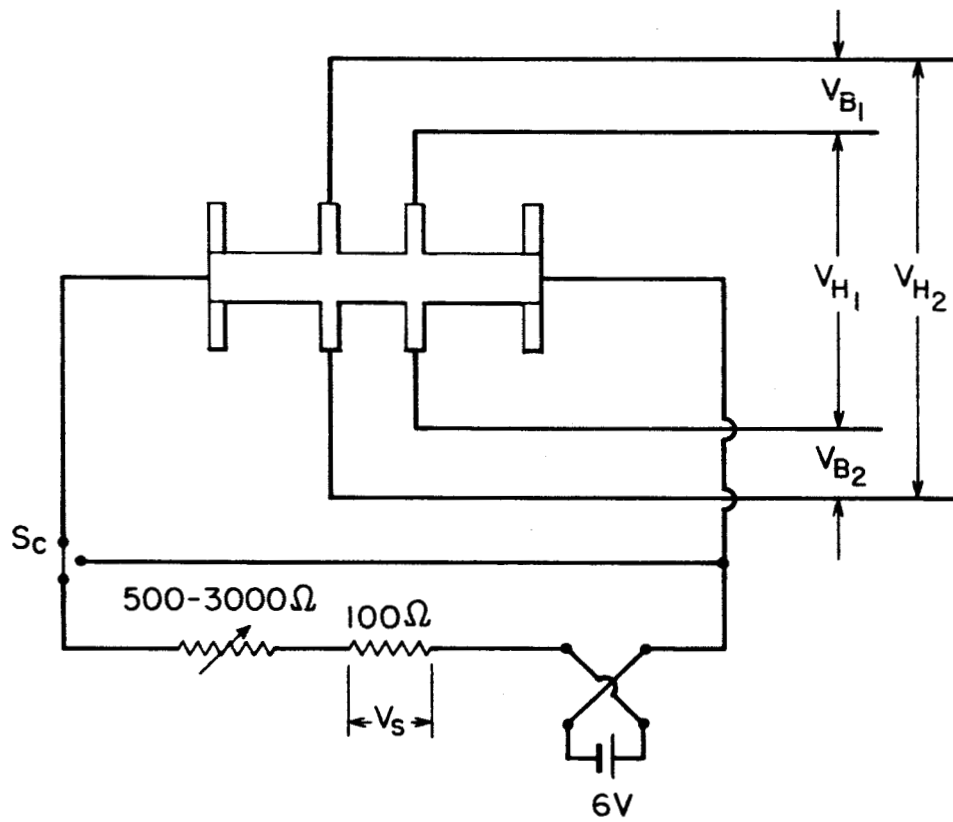
Fig. 3 Circuit diagram for electrical measurements.

specimen and the magnitude of the Hall voltage. If either of these
quantities was high than the higher resistance was used in series.
A 100 ohm standard resistor was used to measure the current in the
circuit.

The Hall voltage, the potential developed across the resistance
leads, the potential across the standard resistor and the thermocouple
e.m.f. were measured with a Leeds and Northrup K3 Potentiometer. When
no measurements were being made, the battery was connected through a
short circuit switch to the resistor in order to minimize the battery
polarization from varying during subsequent measurements.

The Hall coefficient and the resistivity were measured at two pairs
of points of the specimen. In this way the homogeneity of the specimen
and the uniformity of the irradiation could be checked.

3.4 Hall Effect

In designing the specimen for measurements of the Hall coefficient,
the length to breadth ratio was kept larger than 3. This was desirable
because the current electrodes at the ends of the specimen tended to shorten
out the Hall field if the width of the specimen approaches its length.[32]
The width of the electrodes used for measuring the Hall voltage and the
resistivity was kept as small as possible in relation to the width of
the specimen. The width was limited by the low mechanical strength of
the specimen.

In the measurement of the Hall voltage, the spurious voltages arising
from any misalignment on the Hall probes or any temperature gradients in

the specimen had to be avoided. The velocities of the charge carriers
of a given type in a specimen are not all equal, and those carriers with
a lower velocity are deflected more by the magnetic field. As a result,
more energy is transferred to one part of the specimen than the other,
which manifests itself as a temperature gradient. If the specimen
has a high thermoelectric power, an appreciable transverse Ettinghausen-
Seebeck voltage is set up. Its value is given by

$$(V_{E-S})_y = PH_z E_x \Theta \qquad (9)$$

where $(V_{E-S})_y$ is the Ettinghausen-Seebeck voltage in the y-direction,
P is the Ettinghausen coefficient, H_z is the magnetic field in the
z-direction, E_x is the electric field in the x-direction and Θ is the
thermoelectric power of the material.

If a temperature gradient is present in the x-direction, then the
charge carriers will diffuse from the hot to the cold end. In the
presence of a magnetic field this leads to Nernst and Righi-Leduc-Seebeck
voltages across the Hall probes. The Nernst voltage, like the Hall
voltage is created by the Lorentz force on the charge carriers by the
magnetic field, so that this voltage is given by

$$(V_N)_y = Q H_z \left(\frac{dT}{dx} \right) \qquad (10)$$

where $(V_N)_y$ is the Nernst voltage, Q is the Nernst coefficient, and
(dT/dx) is the temperature gradient. The Righi-Leduc-Seebeck voltage,

like the Ettinghausen-Seebeck voltage can therefore be written as

$$(V_{R-L-S}) = SH_z (\frac{dT}{dx}) \theta \qquad (11)$$

where $(V_{R-L-S})_y$ is the Righi-Leduc-Seebeck voltage, and S is the Righi-Leduc coefficient.

In addition to the above three voltages, the misalignment of the Hall probes may give rise to another voltage, which is therefore a resistance drop. Its value is given by

$$(V_\varrho)_y = I_x R \qquad (12)$$

where $(V_\varrho)_y$ is the resistance drop due to the resistance R introduced by the misalignment.

The potential measured across the Hall probes is the algebraic sum of the Hall potential, the Ettinghausen-Seebeck potential, the Nernst potential, the Righi-Leduc-Seebeck potential, and the probe misalignment potential. The last three effects can be eliminated by reversing the magnetic and electric fields so as to obtain a sequence of the following four measurements:

$$V_1 = V_H + V_{E-S} + V_N + V_{R-L-S} + V_\varrho \qquad I_+; H_+ \qquad (13)$$

$$V_2 = -V_H - V_{E-S} + V_N + V_{R-L-S} - V_\varrho \qquad I_-; H_+ \qquad (14)$$

$$V_3 = V_H + V_{E-S} - V_N - V_{R-L-S} - V_\varrho \qquad I_-; H_- \qquad (15)$$

$$V_4 = -V_H - V_{E-S} - V_N - V_{R-L-S} + V_\varrho \qquad I_+; H_- \qquad (16)$$

where V_1, V_2, V_3 and V_4 are the measured potentials across the Hall probes and the subscripts to I and H denote the direction of the current and magnetic fields. By adding equations (13) and (15) and subtracting (14) and (16), the following equation is obtained

$$V_H + V_{E-S} = \frac{V_1 - V_2 + V_3 - V_4}{4} \qquad (17)$$

This equation shows that the Ettinghausen-Seebeck and Hall voltages cannot be separated by the above method. The Ettinghausen-Seebeck effect can be minimized by good thermal contact between the specimen and cryostat so that the thermal gradient is reduced. Alternatively, this voltage can be minimized by allowing the specimen to attain a steady state for a given direction of the current, and then rapidly reversing its direction and making the second measurement before the temperature returns to equilibrium.[10]

3.5 Resistivity

The resistivity of the specimen was measured twice. First, with the direction of current in one direction and second, with the direction of current reversed. The mean value of the sum of the two resistivities was the resistivity of the specimen. The reversal of the current was required to eliminate the effects of temperature gradients.

3.6 Magneto-Resistance

The change in resistance of the specimen on applying a magnetic field can arise not only from a magneto-resistance effect but also from

the presence of thermal gradients as discussed under the Hall effect

measurements, and surface inhomogeneities.   In order to eliminate the

potentials arising from these effects, the magneto-resistance

measurements were made four times with various combinations of the

magnetic and electric fields.   The mean value of the sum of the

potentials measured in this manner was the magneto-resistance potential.

4. Irradiation of Specimens for Electrical Measurements

The specimen holder containing the specimen was placed on the

water cooled target holder, as shown schematically in Figure 4.   The

target holder was made of copper.   The specimen holder was held in

place firmly against the target holder by two screws.   The whole

assembly was placed in the evacuated internal beam chamber of the

cyclotron.

The desirable level of proton beam current in the cyclotron was

determined by trial and error in the following manner.   A specimen was

irradiated with a given beam current to a specified integrated dosage.

Changes in the Hall coefficient and resistivity caused by the irradiation

were measured.   Another specimen was then irradiated at a lower beam

current up to the same integrated dose.   Changes in the Hall coefficient

and resistivity caused by the irradiation were again measured.   This

procedure was continued until the changes in the electrical properties

were observed to be relatively insensitive to the changes in the level of

the beam current.   The largest value for which this was observed was
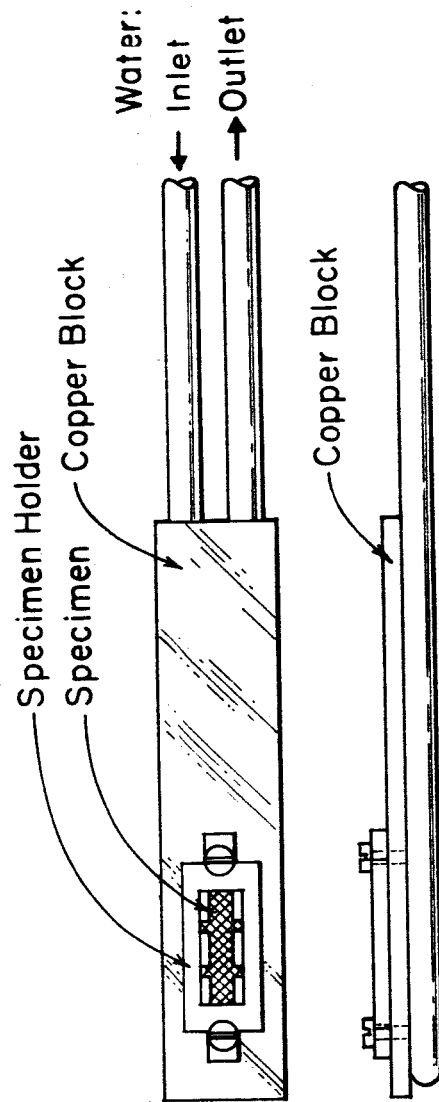
Fig. 4 Water cooled target holder for irradiating specimens for electrical measurement.

used as the operating beam current. This current was 1.0×10^{12} protons per cm^2 per sec. The use of a higher beam current caused an excessive temperature rise in the specimen and probably annealed out the defects introduced by the irradiation.

The flux of protons incident on the specimen was determined by determining the distribution of the proton beam in the plane of the target holder. This determination was made in an auxiliary run in which a test paper was irradiated at a low beam current. Because of the approximate nature of the determination of this distribution, the value of the flux may have been in error as much as 20 or 30 pct of the reported value.

5. Specimens for Examination by Electron Microscopy

Single crystals of the compound Bi_2Te_3 were heat treated in vacuum or under an atmosphere of argon at $350^{\circ}C$ for 24 hours in the manner described in Section IV, 2.1. After this heat treatment one surface of the crystal was cleaved with Scotch tape.

The electron microscopy specimens were prepared from this crystal by joining the freshly cleaved surface of the crystal to a microscope slide with Duco cement. After the Duco cement had set, the specimen was cleaved with Scotch tape until no further cleaving was possible. The part of the specimen which still adhered to the slide was removed from it by dissolving the cement in acetone. The specimen was

collected on an electron microscope grid of 75 mesh size. The grid was then folded over the specimen in order to hold it securely in place. Specimens prepared in this manner were examined under the electron microscope before irradiation and only those which were sufficiently thin for transmission electron microscopy were selected.

6. Examination of Specimens by Transmission Electron Microscopy

The defect structure introduced by irradiation can be observed in the electron microscope because of diffraction contrast effects. The diffraction contrast between the region immediately surrounding the defect and the matrix arises from the distortion of the lattice planes in the vicinity of the defect.

By suitably inclining the specimen with respect to the electron beam the lattice planes near the defect can be made to diffract the electrons. This reduces the number of transmitted electrons and the diffracting region appears as a dark area relative to the surrounding area. If the operating reflection is varied systematically around the origin in reciprocal space, the direction of the strain can be determined. Following Hirsch et al.[33] the condition in which no diffraction contrast is observed can be stated as

$$\vec{g} \cdot \vec{b} = 0 \qquad (18)$$

where $\bar{g}$ is the reciprocal lattice vector corresponding to the operative

reflection and $\bar{b}$ is the Burgers vector. In order to determine the

direction of the Burgers vector, it is necessary to choose a reflection

for which the condition expressed by equation (18) is satisfied. Such

a reflection can be produced by gradually tilting the specimen to obtain

the operative Bragg reflection. The wave length of 100 kv electrons is

0.037 A.U. so that the angles over which the specimen has to be tilted

in order to obtain a different reflection is usually less than a

degree. In the Siemens Elmiskopp I microscope a specimen can be tilted

by the use of a "double tilt" specimen holder. This holder permits the

specimen to be tilted about two axes perpendicular to each other and to

the electron beam. The Hitachi HU-11 microscope has a single tilt

for room temperature operation, but has no tilt facilities for the low-

temperature stage.

Contrast effects can also be observed under the electron microscope

in regions of the specimen that have different absorption coefficients

or different thickness. Contrast due to either of these causes can

be distinguished from diffraction contrast by dark field microscopy.

In an investigation of clusters of point defects the use of dark-field

microscopy is advantageous.[26,34] The nature of the defect structure

can be identified in those cases in which dynamical effects are important

and the simple kinematical theory of diffraction is not applicable.

7. <u>Irradiation of Specimen for Examination by Electron Microscopy</u>

While the target holder for irradiating specimens for electrical measurements accommodated only one specimen, the target holder arrangement shown in Figure 5 held up to five specimens. An aluminum foil of thickness 5×10^{-4} cm was used to keep the grids pressed against the surface of the water cooled aluminum block.

This method of irradiating specimens for electron microscopy also differed from the one used for irradiating the specimen for electrical measurements in the following ways: (1) The foil pressing the grids against the block reduced the energy of the protons reaching the surface of the specimen;   (2) The specimens for the electron microscope were not cooled uniformly during irradiation because the heat had to be transferred through the mesh of the grids since there was no other direct path from the specimen to the block on one side and the foil on the other. The areas in direct contact with the metal in the mesh were cooled more efficiently than areas facing the openings.
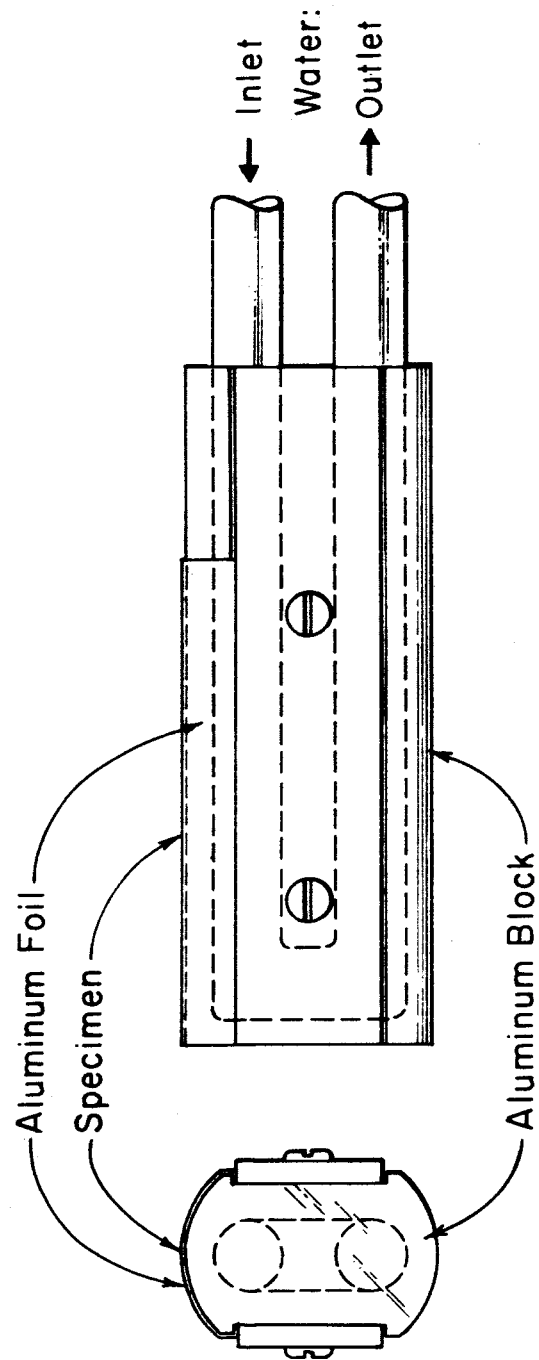
Fig. 5 Water cooled target holder for irradiating specimens for electron microscopy.

Water:
Inlet
Outlet

Aluminum Foil
Specimen
Aluminum Block

V.   RESULTS

1.   Electrical Measurements

The electrical properties of the compound Bi_2Te_3 before and after successive irradiations were measured as a function of temperature. The measurements were carried out over the range of temperature from $82^\circ K$ to room temperature. The integrated radiation doses ranged from 1.0×10^{15} to 1.5×10^{16} protons per cm^2. After preliminary work with several specimens, three of the specimens were carried through complete cycles of successive irradiations and measurements. The results reported here are for one of the three specimens and are representative of the other two specimens.

1.1 Hall Coefficient

In Figure 6 the Hall coefficient has been plotted as a function of temperature after successive irradiations. The integrated radiation doses are stated in the figure. The Hall coefficient of the unirradiated specimen measured as a function of temperature is in good agreement with published values.[8,10] The specimens became intrinsic at about $290^\circ K$. This is in accord with the values of the energy gap of 0.16 to 0.21 ev stated in the literature.[10]

After successive irradiations the Hall coefficient increased. Below a total radiation dose of about 4.6×10^{15} protons per cm^2, the Hall coefficient measured as a function of temperature showed a slight increase in the vicinity of $240^\circ K$ similar to the unirradiated specimen. With
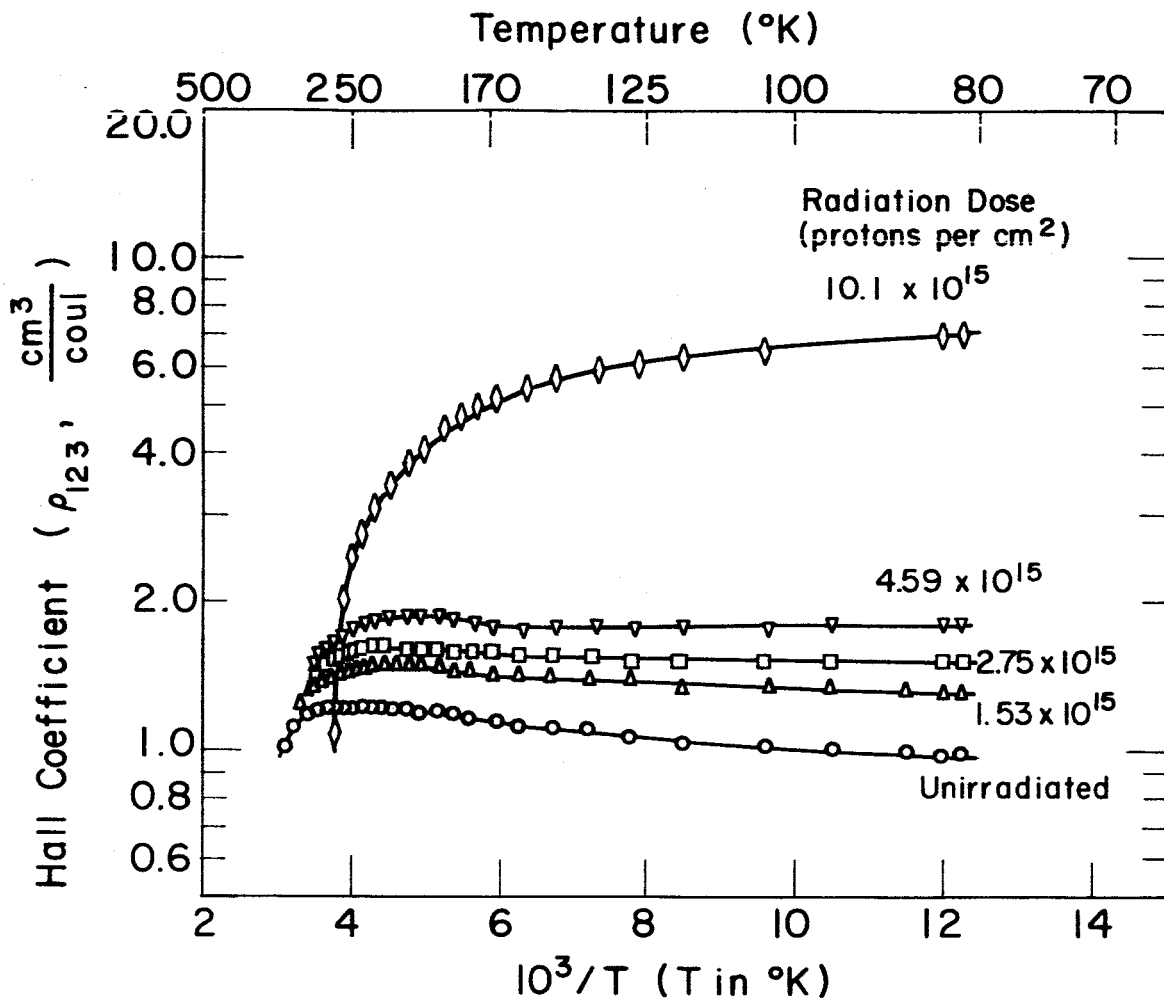
Figure 6 Hall coefficient as a function of temperature after successive irradiations.

increasing successive irradiations the specimen became intrinsic on heating at lower temperatures. After irradiation to doses larger than 4.6×10^{15} protons per cm^2 the slight increase in the Hall coefficient as a function of temperature observed with low doses and unirradiated specimens was not observed. This was due to the onset of intrinsic behavior at lower temperatures. After an integrated dose of 1.2×10^{16} protons per cm^2, the specimen was converted from p-type to n-type.

The change in the Hall coefficient with temperature after successive irradiations shows that the predominant type of defects introduced by irradiation are donors, and that these defects are ionized at $82^{\circ}K$. Defects are expected to be created by proton irradiation as a result of both replacement and displacement collisions between the protons and atoms of bismuth and tellurium. On the basis of the hydrogenic model the defects are expected to be ionized in this compound at $82^{\circ}K$.[1]

1.2 Electrical Resistivity

In Figure 7, the electrical resistivity of the unirradiated and irradiated specimen is given as a function of temperature after successive irradiations. Between 175 and $280^{\circ}K$ the change in the resistivity of the unirradiated specimen with temperature can be represented by

$$\rho_{11} = 5.19 \times 10^{-8} \, T^{1.98} \tag{19}$$

This change in resistivity with temperature is in good agreement with the published values for the unirradiated specimen.[8]
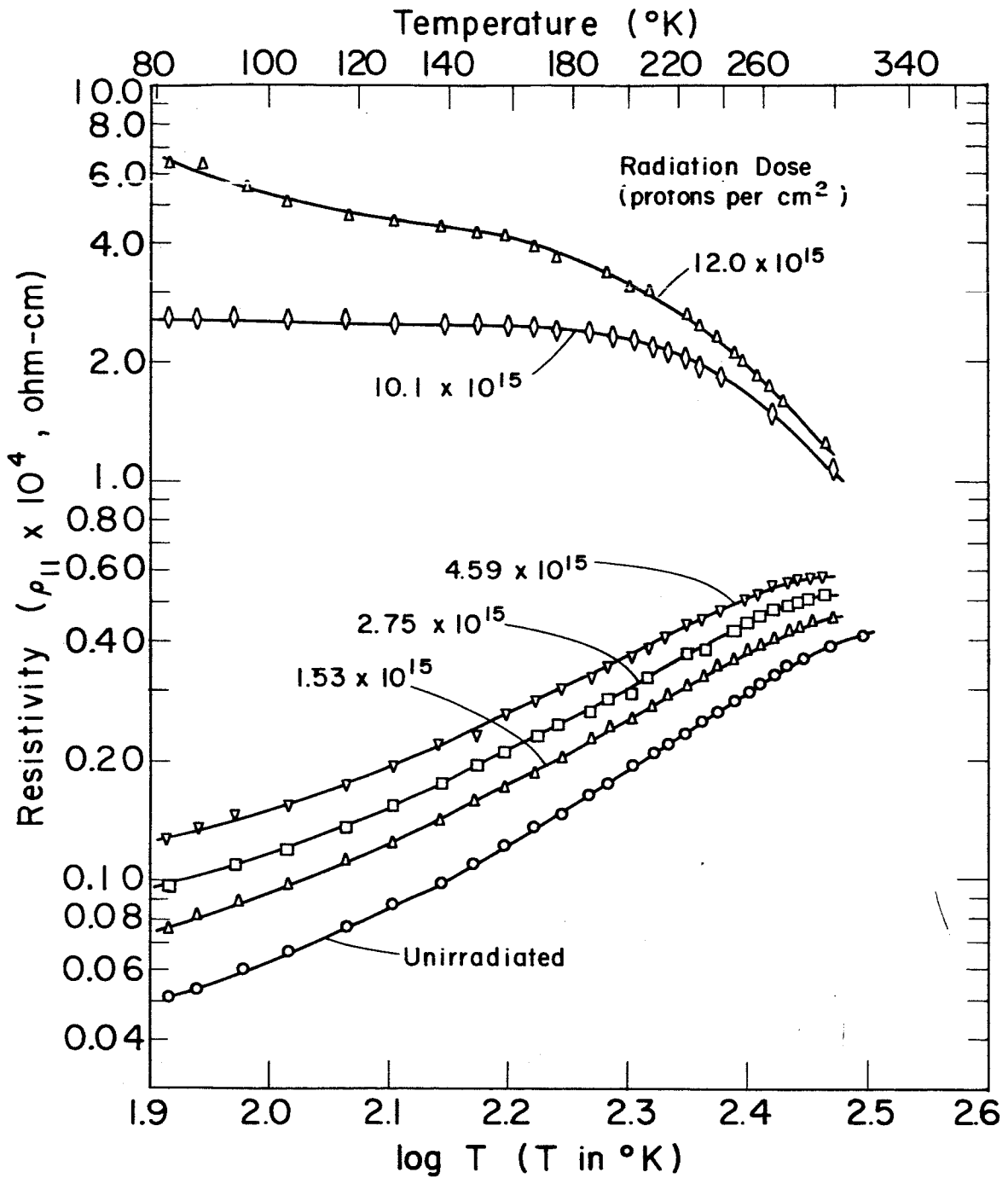
Figure 7 Resistivity as a function of temperature after successive irradiations.

On irradiation the resistivity increased. The exponent of the temperature dependence of the resistivity decreased and became negative after the highest integrated dose used. Such an increment in resistivity with irradiation can be explained if the number of carriers decreases and the effect of defect scattering by charged defects becomes more marked with increasing irradiation dosage.

1.3 Hall Mobility

The ratio of the Hall coefficient and resistivity which is defined as the Hall mobility, has been plotted in Figure 8 as a function of temperature after successive irradiations. Between 220 and $280^{\circ}K$ the change in the Hall mobility of the unirradiated specimen with temperature can be represented by

$$\mu_H = 3.39 \times 10^7 \, T^{-2.04} \tag{20}$$

The significance of this relation is not clear, particularly since the Hall coefficient of the unirradiated specimen is known to increase anomalously in this temperature range. Drabble[8] has suggested that the resistivity relation of the type shown by equation (19) is more representative of mobility than the Hall mobility. In Figure 9, the Hall mobility and resistivity measured at $82^{\circ}K$ have been plotted as functions of the radiation dosage. An increase in the dosage is associated with a decrease in the Hall mobility and an increase in the resistivity.
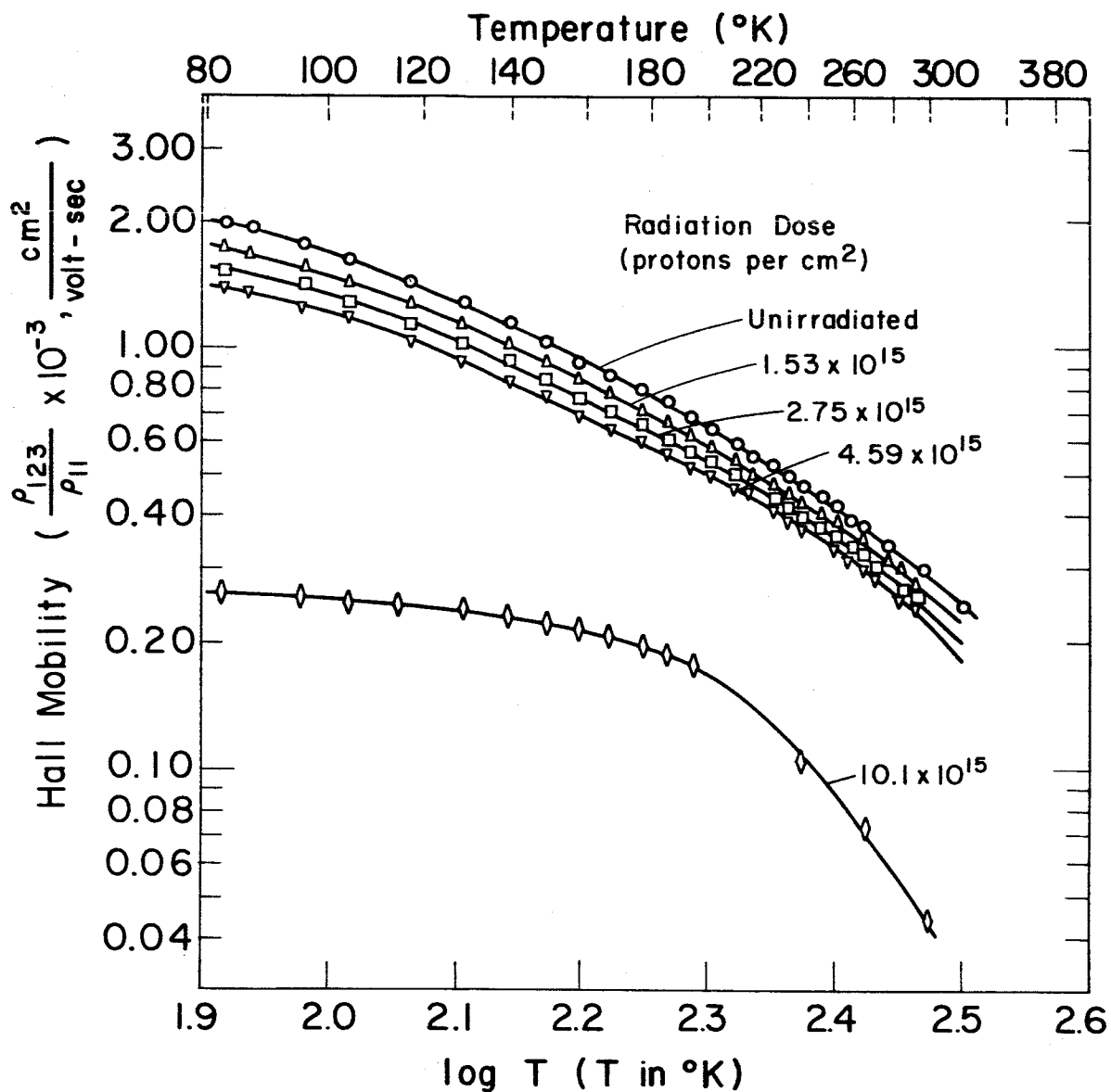
Figure 8 Hall mobility as a function of temperature
after successive irradiations.

40
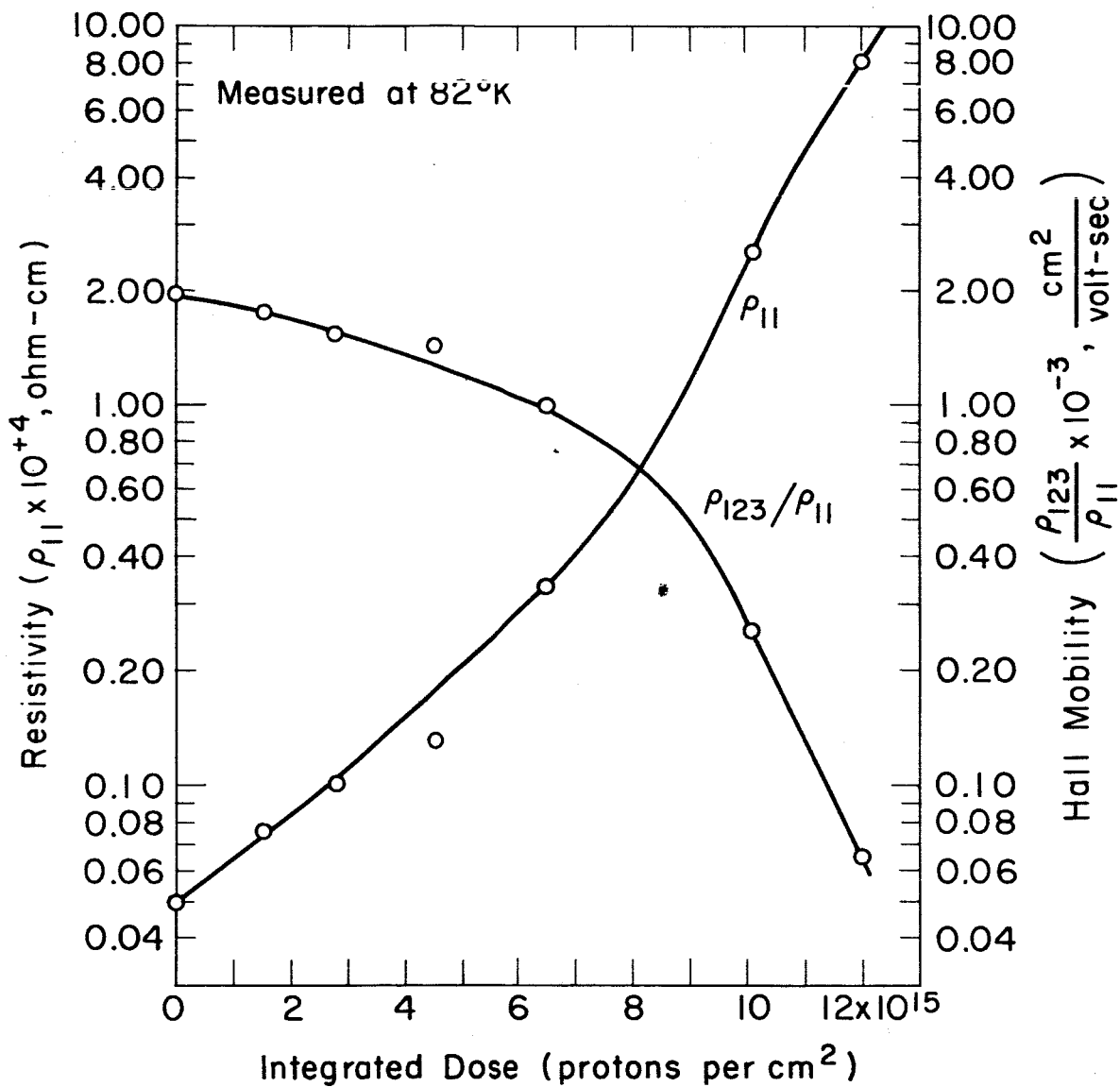
Figure 9. Resistivity and Hall mobility as functions of integrated radiation dose.

41

1.4 Coefficient of Magneto-resistance

In Figure 10 the fractional increase in resistance measured at $82^{O}K$

on applying a magnetic field has been plotted against the square of

the magnetic field.   A straight line is obtained after all integrated

radiation dosages investigated.   The slope of the line gives the

coefficient of magneto-resistance; it has been plotted in Figure 11

as a function of the radiation dosage.   With increasing irradiation

the coefficient of magneto-resistance decreases with increasing integrated

dosage and appears to reach a limiting value after an integrated dose of

1.0×10^{16} protons per cm^2.

2. Transmission Electron Microscopy

Specimens of the compound Bi_2Te_3 were examined before and after

irradiation.   Two batches containing several specimens each were

irradiated at two levels of flux of protons for the same integrated dose.

This dose was 5.5×10^{18} protons per cm^2, which was two orders of

magnitude larger than for the specimens on which the electrical

measurements were made.   This difference in radiation dose was

necessary because the point defect clusters after an integrated dose of

10^{16} protons per cm^2 were not expected to be sufficiently large and

sufficiently numerous for examination by transmission electron microscopy.

The orientation of the foils was determined by electron diffraction.

The diffraction pattern of the selected area and the bright field image
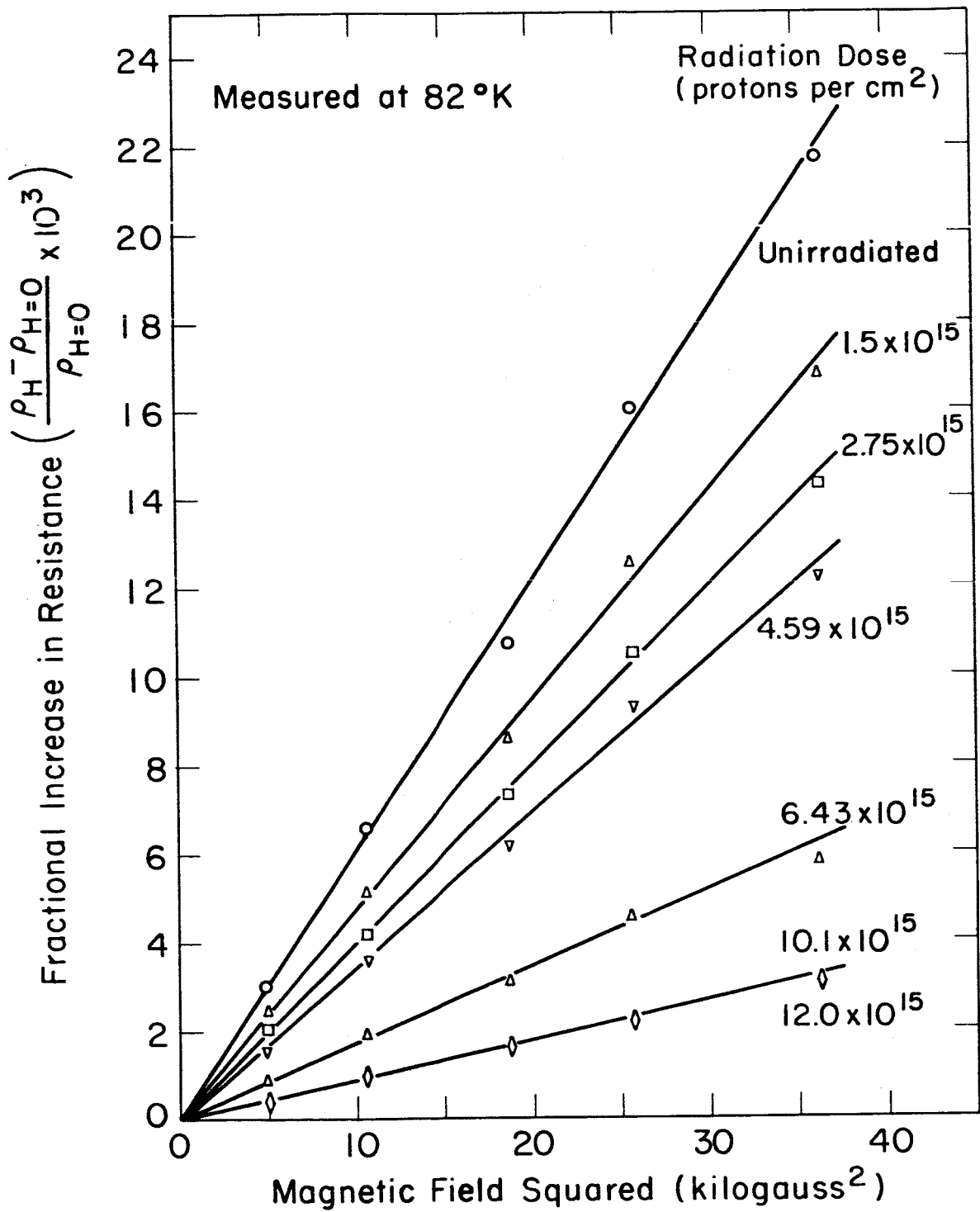
Figure 10. Fractional increase in resistance as a function of the square of the magnetic field after successive irradiations.

43
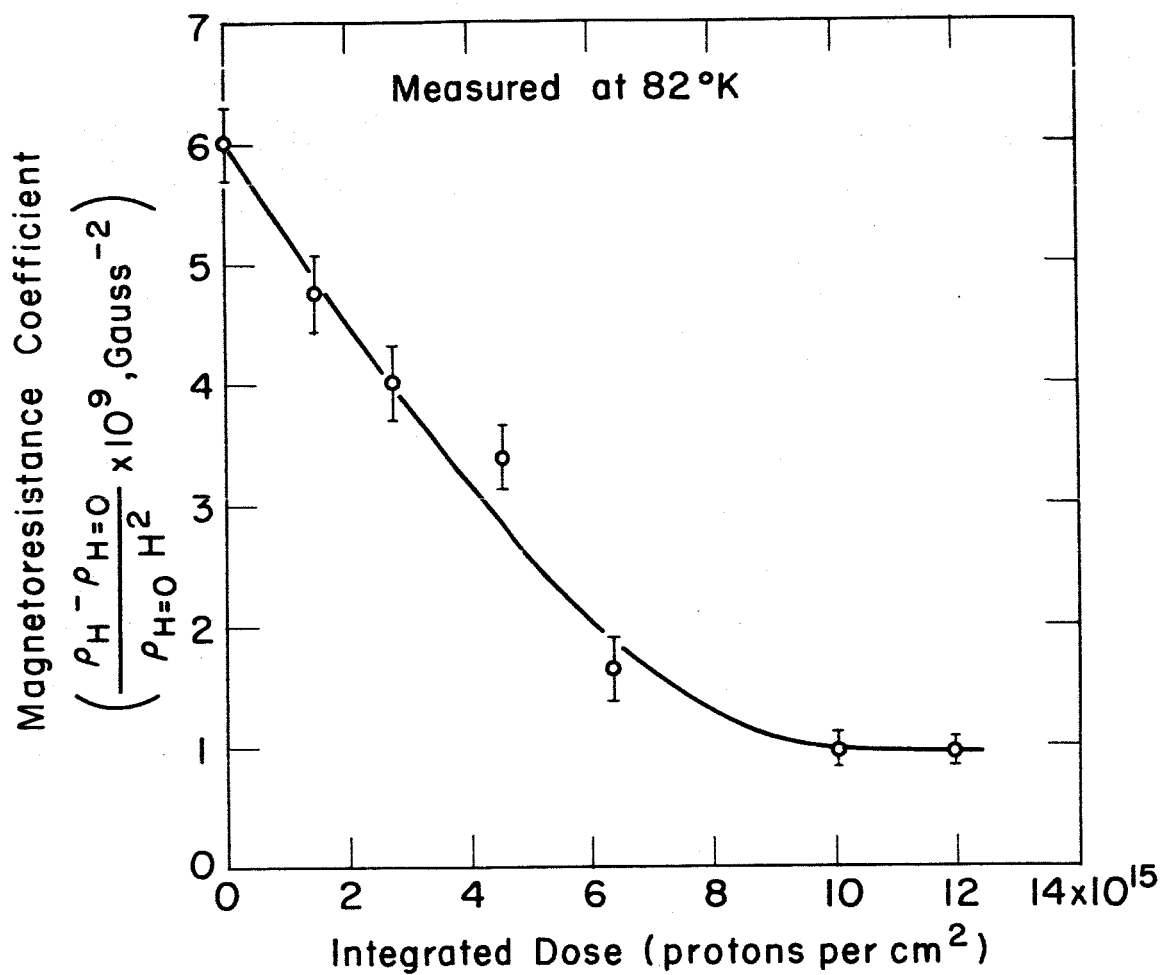
Figure II. Magnetoresistance coefficient as a function of
integrated radiation dose.

corresponding to this selected area were rotated with respect to each other through the required angle to eliminate the rotation of the image relative to the diffraction pattern.

The range of magnification of the electron micrographs was between 15,000 and 30,000 diameters. These micrographs were further enlarged to magnifications ranging from about 40,000 to 70,000 diameters.

2.1 Point Defects

2.1.1 Irradiation with a Low Flux of Protons - The flux was 1.8×10^{13} protons per cm^2-sec and the integrated dose was 5.5×10^{18} protons per cm^2. Irradiation introduced point defect clusters ranging in size from 50 to 250 A.U. These clusters can be seen as dark spots in Figures 12 and 13. The orientation of the foil in the electron microscope was such that the c-axis of the specimen was parallel to the electron beam of the microscope. In this orientation some of the defects are observed to be aligned along the $\langle 10\bar{1}0 \rangle$ and $\langle 11\bar{2}0 \rangle$ directions. In Figure 12(a), some of the area corresponding to these configurations have been marked A and B.

The point defect clusters were observed under the electron microscope to anneal out, presumably because of the heat generated by the electron beam of the microscope. The annealing out is shown by the two sequences of electron micrographs in Figures 12(a)-(d) and 13(a)-(c). The micrographs in Figure 12 were taken after approximately thirty second intervals. In the micrographs in Figure 13, some of the defect clusters can be seen to anneal out during the time required to align the microscope

Figure 12. Defect clusters in proton irradiated Bi_2Te_3. Electron micrographs taken after approximately thirty second intervals. Areas marked A and B show some of the defect clusters aligned along the $\langle 10\bar{1}0 \rangle$ and $\langle 11\bar{2}0 \rangle$ directions, respectively. The dislocation marked C remains unchanged; the dislocation marked D reduces its length. The length of the mark equals 2,000 A.U. Flux level equals 1.8×10^{13} protons per cm^2-sec. Integrated dose 5.5×10^{18} protons per cm^2.
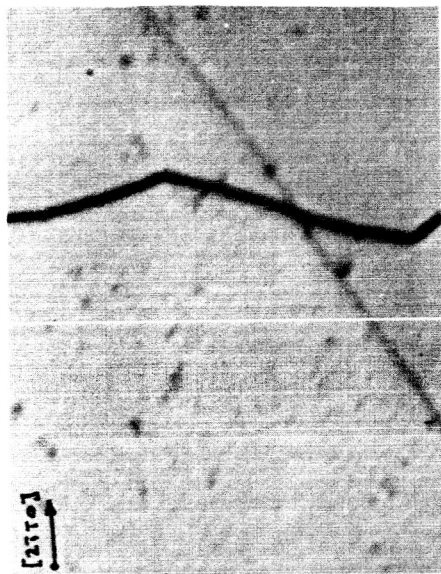
(a)
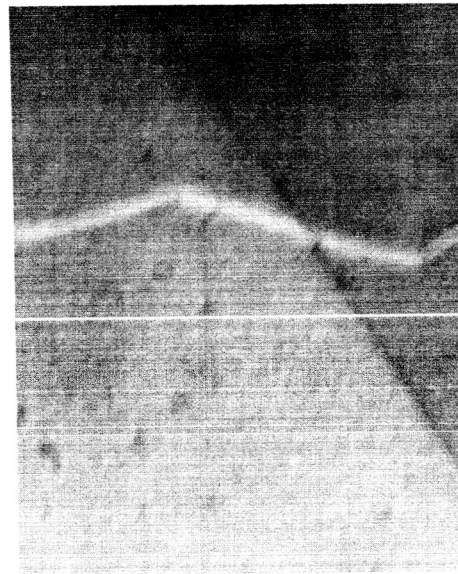
(b)
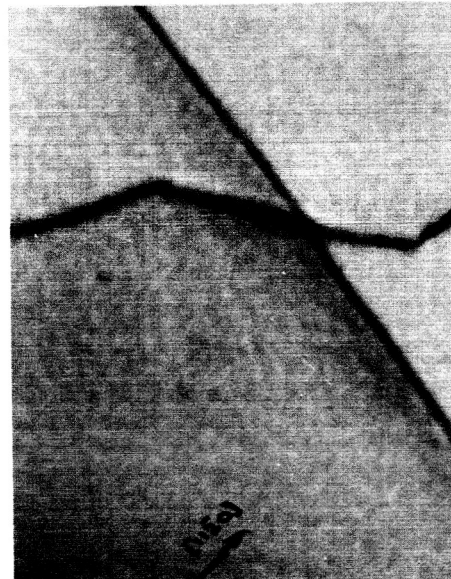
(c)

Figure 13. Defect clusters in proton irradiated Bi_2Te_3. The length of the mark equals 2,000 A.U. Flux level equals 1.8×10^{13} protons per cm^2-sec. Integrated dose 5.5×10^{18} protons per cm^2.

(a) Bright-field image corresponding to a $(2\bar{1}\bar{1}0)$ type reflection.

(b) Dark-field image of (a). Some of the defect clusters have annealed out.

(c) Bright-field image corresponding to a $(11\bar{2}0)$ type reflection. All defect clusters have annealed out.

47

for dark field microscopy. During subsequent realignment for bright field microscopy and tilting the specimen to obtain a different diffraction vector, the defect clusters had annealed out. Two specimens were also examined at the temperature of liquid nitrogen. Dark spots similar to the ones shown in the micrographs in Figures 12 and 13 were observed. These spots were not observed to anneal out during the time the specimens were in the microscope.

2.1.2 **Irradiation with a High Flux of Protons** - The flux was 3.0×10^{13} protons per cm^2-sec. and the integrated dose was 5.5×10^{18} protons per cm^2. The defect clusters present after the irradiation with a flux of 1.8×10^{13} protons per cm^2-sec. shown in the micrographs in Figures 12 and 13 were not observed. They may be assumed to have annealed out during irradiation because of the rise in temperature arising from the higher flux. A different type of defect cluster was, however, observed. An example is shown in the sequence of micrographs in Figure 14.

The defect clusters marked I in Figures 14(a) and (b) show a line of no contrast perpendicular to the diffraction vector. This line of no contrast corresponds to the condition given by equation (18). The symmetry line cutting across the two crescents is parallel to the diffraction vector in Figure 14(a) and (b). This indicates that the strain field of this defect is symmetrical about the c-axis.
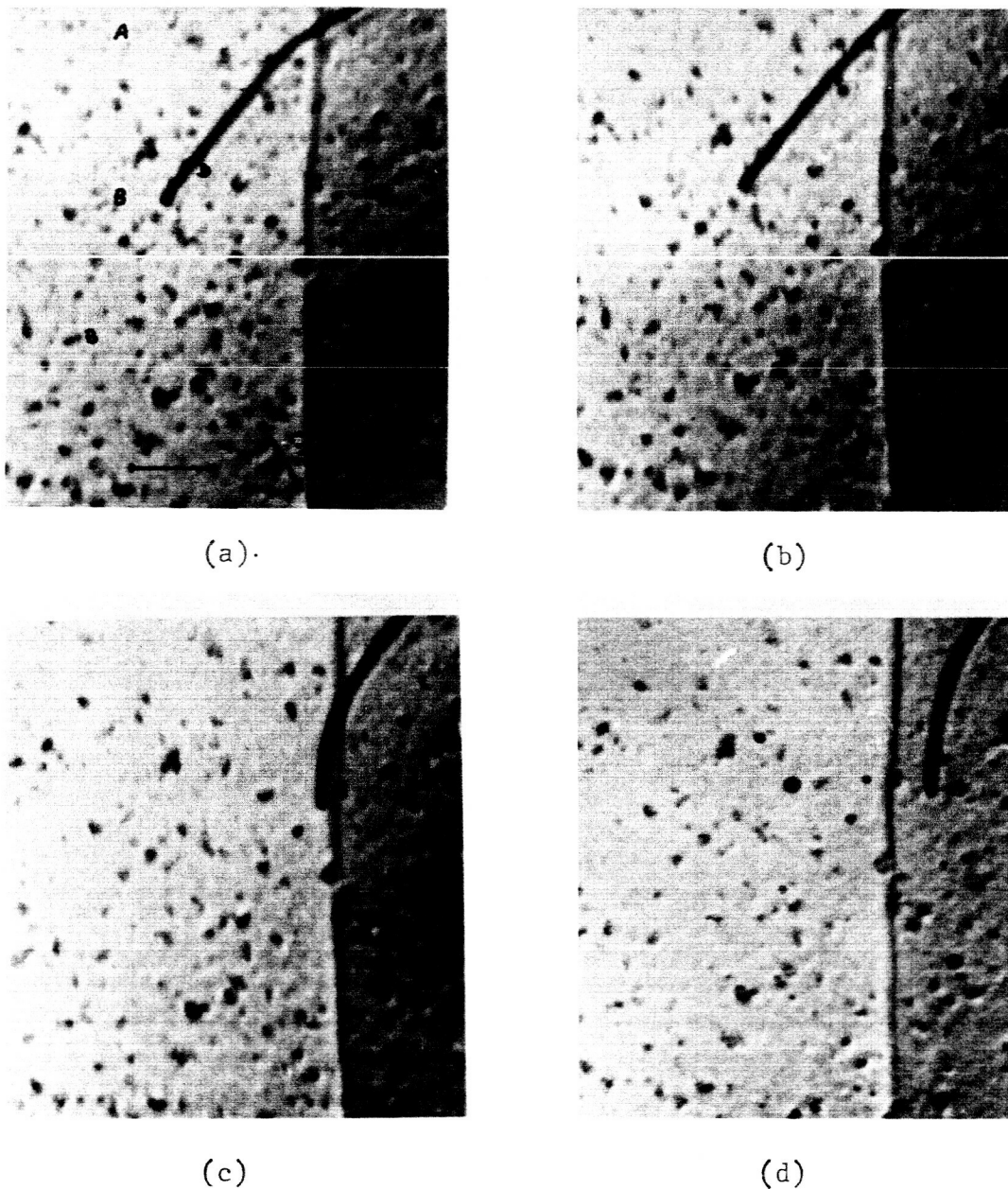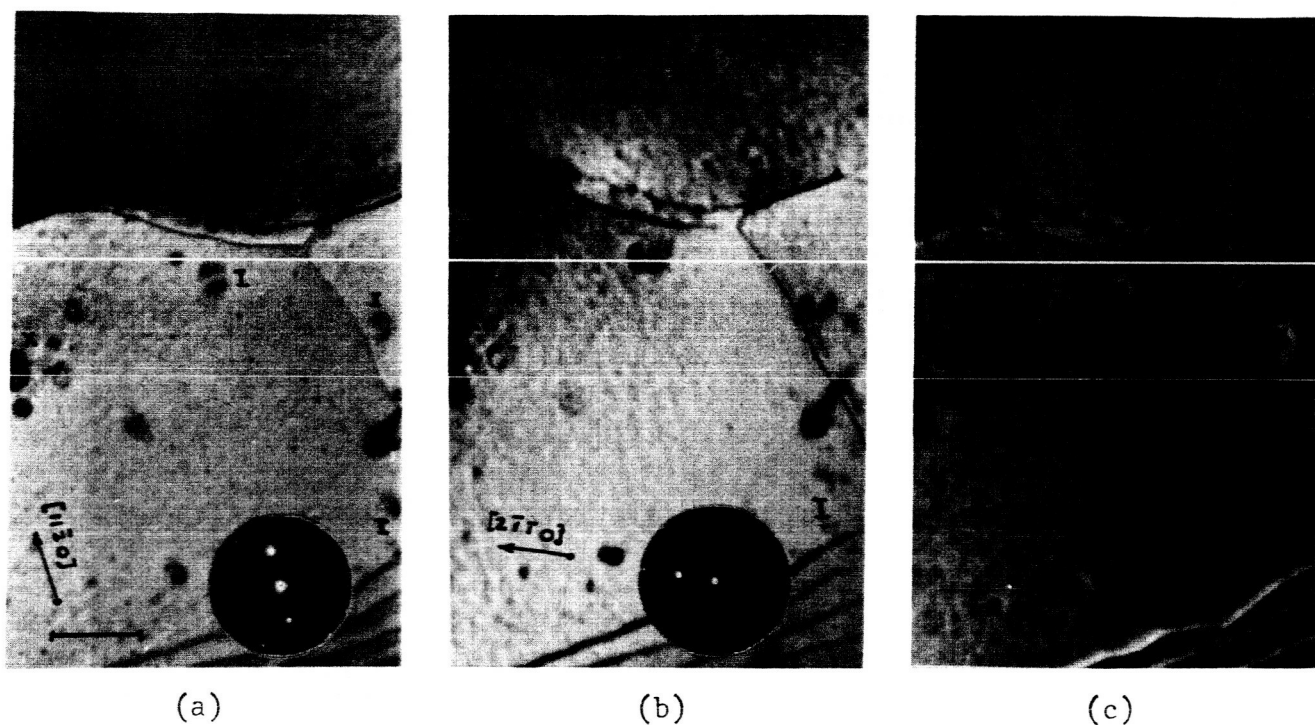
Figure 14. Defect clusters in proton irradiated Bi_2Te_3. Electron
micrographs taken for two different diffraction vectors.
The length of the mark equals 2,000 A.U. Flux level
equals 3.0×10^{13} protons per cm^2-sec. Integrated dose
5.5×10^{18} protons per cm^2.

(a) Bright-field image corresponding to a reflection
from $(11\bar{2}0)$ type planes. The line of no contrast
of the defect clusters marked I is normal to the
diffraction vector.

(b) Bright-field image corresponding to a reflection
from $(2\bar{1}\bar{1}0)$ type planes. The line of no contrast
in the defects marked I has rotated so that it is
normal to the diffraction vector.

(c) Dark-field image of (b). Note that the light side
of the image from the clusters is in the opposite
direction for the defect clusters marked I and V.

The micrograph in Figure 14(c) is the dark field image of the micrograph in Figure 14(b). On applying the results of an analysis of Ashby and Brown[35] the spots marked I and V can be identified as clusters of interstitials and clusters of vacancies.

In some areas of some of the specimens investigated, effects of the type shown in Figure 15 were observed. They were aggregates of light and dark regions and small light regions having hexagonal symmetry. When the beam current of the microscope was slowly increased so as to raise the temperature of the specimen, the hexagonal areas, for example, areas marked B, were observed to grow. This is seen in the sequence of electron micrographs in Figure 15(a)-(c). The small light spots were also observed to grow into the larger areas with hexagonal shapes, for example, the area marked C. Some of the hexagonal areas were observed to assume triangular shapes. An example of this is shown in the area marked A in the micrographs in Figure 15(a), (b), and (c). The sides of the hexagonal areas and of the triangular areas were parallel to one of the $\langle 11\bar{2}0 \rangle$ directions.

2.2 Dislocations

Dislocations were present in the specimens as a result of the stresses involved in their preparation. Irradiation with protons is believed not to generate new dislocations, but may alter their arrangement. The heating by the electron beam causes further changes in the arrangement of dislocations as well as interaction between dislocations and point defect clusters.

(a)

(b)

(c)
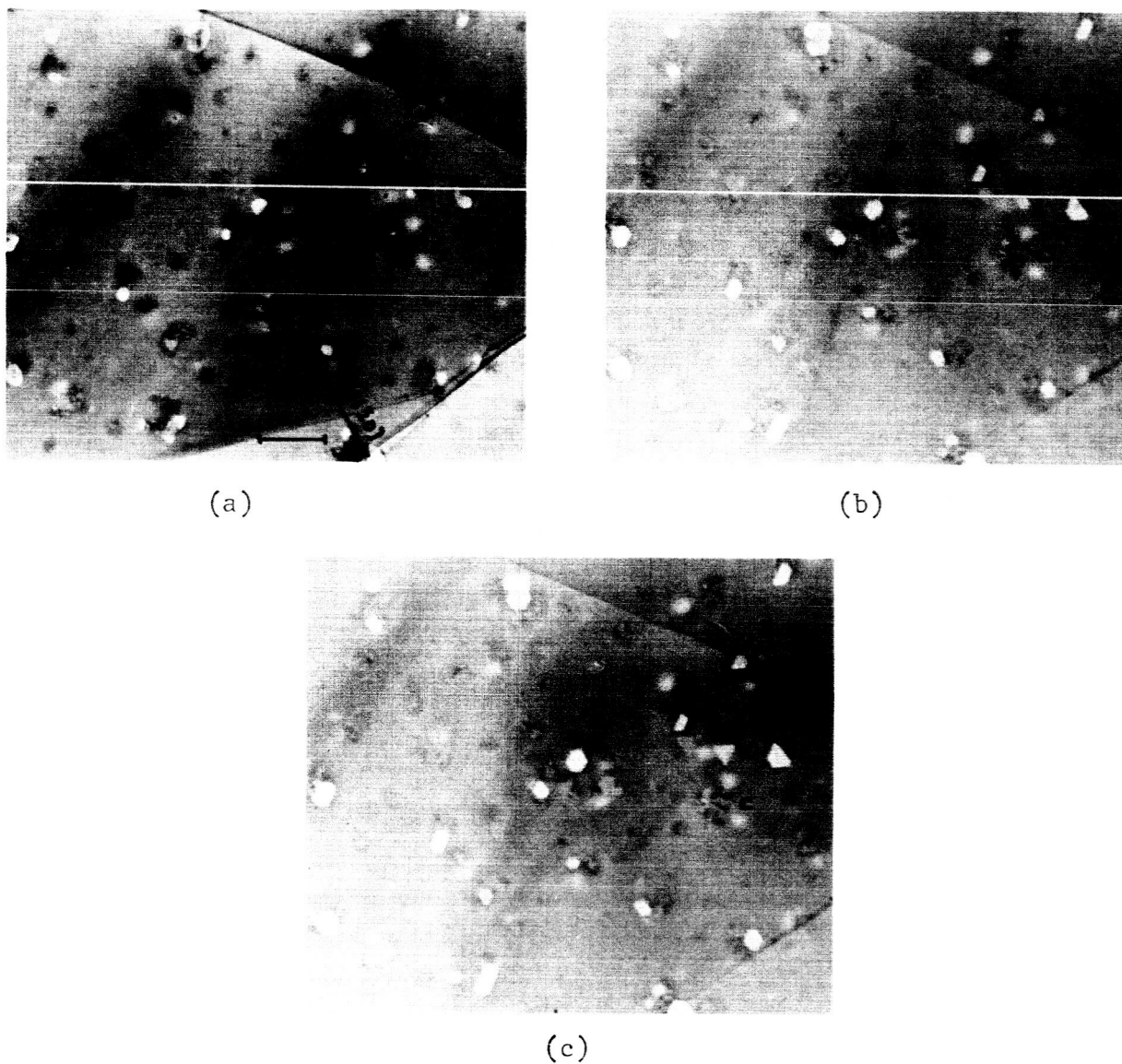
Figure 15. Growth of hexagonal areas during observation in the
electron microscope in proton irradiated Bi_2Te_3.
Areas marked A, B, and C show these areas growing
with time. In the area marked A the hexagonal areas
have assumed triangular shapes. The sides of the
hexagonal and triangular areas are parallel to
$\langle 11\bar{2}0 \rangle$ directions. The length of the mark equals
2,000 A.U. Flux level equals 3.0×10^{13} protons
per cm^2-sec. Integrated dose 5.5×10^{18} protons
per cm^2-sec.

The effect of irradiation on dislocations can be seen in the micrographs in Figures 12, 13, 14, and 16. After irradiation the dislocation lines frequently contained segments which showed no diffraction contrasts. An example of this is the segment marked S of the dislocation in the micrograph in Figure 16. This micrograph also illustrates the effect of irradiation on a dislocation network. The dislocation lines forming the network are broken and intersect the surface of the specimen at such points as P.

During observation in the microscope these dislocations, one end of which intersects the surface, reduce their length. An example of this is the dislocation marked D in the sequence of micrographs in Figure 12(a)-(d). Similar observations of dislocation movement in the microscope have been reported on unirradiated specimens of Bi_2Te_3.[7]

In the unirradiated specimens, the dislocation lines are smooth and generally tend to be parallel to each other. After irradiation these lines become jagged although they are still approximately parallel to each other. This can be seen in the micrographs shown in Figures 14(c) and 16.

Figure 16. Effect of proton irradiation on dislocation and dis-
location networks. The dislocation line is out of
contrast at the segment marked S. The length of the
mark equals 2,000 A.U. Flux level equals 1.8×10^{13}
protons per cm^2-sec. Integrated dose 5.5×10^{18}
protons per cm^2.

53

VI. DISCUSSION

1. Electrical Measurements

On the basis of the multivalley band structure proposed for the compound Bi_2Te_3, the magneto-resistance tensor ς_{1133} is given by[8]

$$\varsigma_{1133} = \frac{\varsigma^2_{123}}{\varsigma_{11}} \left[\frac{(1 + u)^2}{4 u \beta} - 1 \right] \qquad (21)$$

In this expression ς_{123} is the Hall coefficient, ς_{11} is the resistivity, u is equal to α_{22}/α_{11}, where α_{22} and α_{11} are two of the four coefficients that describe the shape of the valleys in k-space, and β is the ratio of the transport integrals $I_1^2 / I_0 I_2$, where the integral I_n is given by

$$I_n = - \left(\frac{e}{m}\right)^n \frac{e^2}{3\pi^2 m} \left(\frac{2m}{h^2}\right)^{3/2} \frac{1}{\Delta^{1/2}} \int \tau^{n+1} E^{3/2} \frac{\delta f_o}{\delta E} dE \qquad (22)$$

In this equation m is the free electron mass, e is the electronic charge, h is Planck's constant, Δ is the determinant of the tensor α_{ij}, τ is the relaxation time, f_o is the equlibrium Fermi-Dirac distribution function, and the integral is evaluated over the energy states associated with a single valley.

Equation (21) can be rearranged to give

$$\left(\frac{\varsigma_{1133} \varsigma_{11}}{\varsigma^2_{123}}\right) = \left[\frac{(1 + u)^2}{4 u \beta} - 1 \right] \qquad (23)$$

The value of the ratio of the quantity on the left side of this
equation can be found from the experimentally determined values of
ρ_{11}, ρ_{123} and ρ_{1133}. It has been plotted as a function of the integrated
radiation dosage in Figure 17. Within the limits of experimental error
the quantity given by the left hand side of equation (23) is observed
to be approximately independent of the integrated radiation dosage
up to a dose of 1.0×10^{16} protons per cm^2. After a dose of 1.2×10^{16}
protons per cm^2 the material is converted from p-type to n-type and
therefore a change in the band structure parameters is expected. It can
be concluded that for integrated doses less than 1.0×10^{16} protons per
cm^2 the band structure of the compound Bi_2Te_3 does not change. The
Hall coefficient and resistivity data can therefore be analyzed on the
basis that α_{11} and α_{22} remain constant under irradiation.

1.1 Hall Coefficient

The Hall coefficient is given by[8]

$$\rho_{123} = \frac{4u}{(1+u)^2} \frac{1}{pe} \tag{24}$$

where p is the number of holes per cm^3 and e is the electronic charge.
Substituting for u the value obtained by Drabble[8], equation (24) can
be written as

$$\rho_{123} = \frac{0.514}{pe} \tag{25}$$
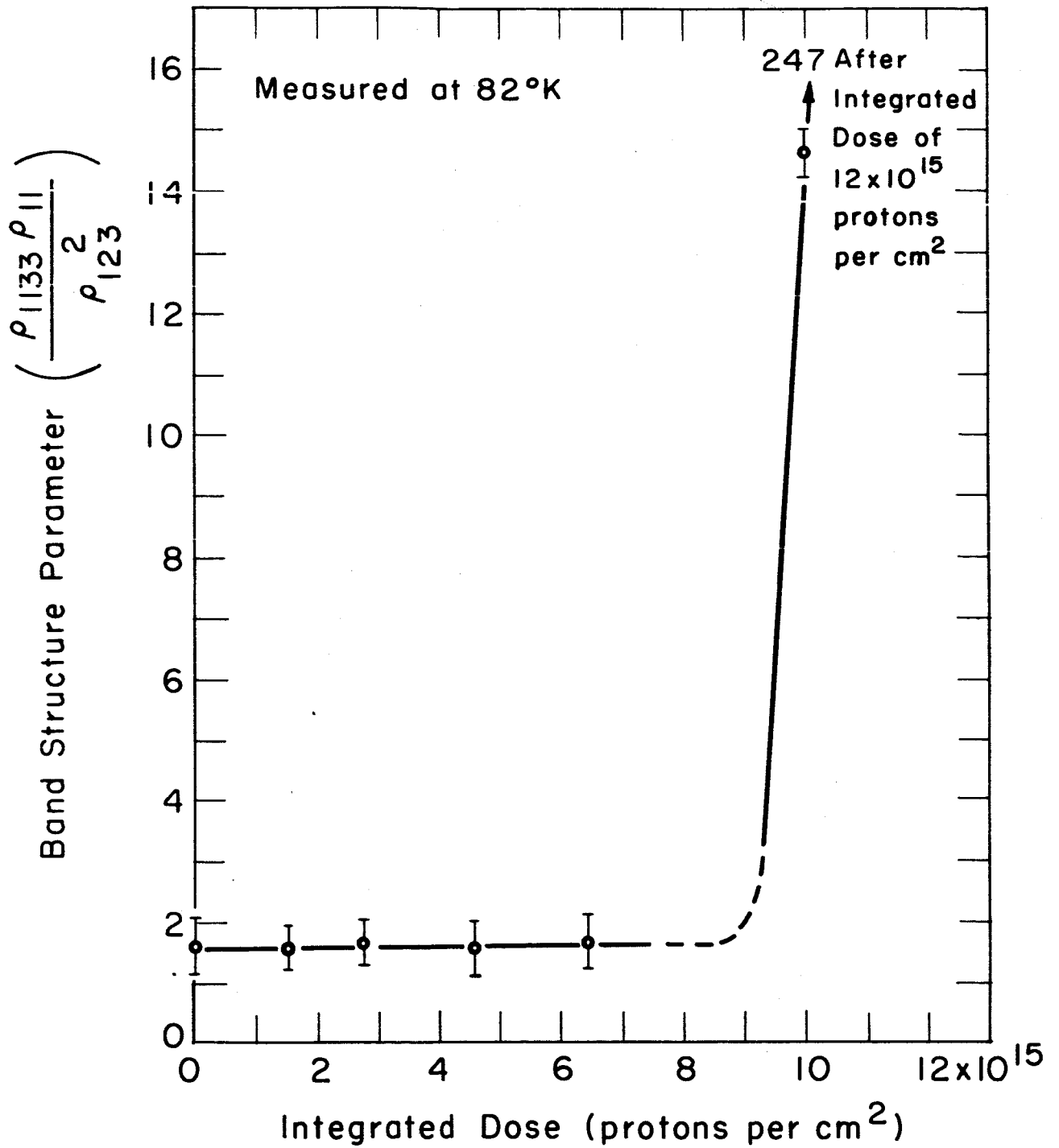
Figure 17.   Band structure parameter as a function of
integrated radiation dose.

The number of holes per cm^3 is also related to the Fermi energy by the expression

$$p = \frac{4\pi(2m^* kT)^{3/2} F_{1/2}(\eta^*)}{h^3} \qquad (26)$$

where m^* is the effective mass of the holes and $F_{1/2}(\eta^*)$ is the Fermi-Dirac integral of order one half. After substituting for p and rearranging, equation (25) gives

$$F_{1/2}(\eta^*) = \frac{0.514 \, h^3}{4\pi e (2m^* kT)^{3/2} \, \mathcal{Q}_{123}} \qquad (27)$$

The values of the constants in this equation are known and, if $m^* = 0.511 \, m^{(8)}$ is assumed to hold for the specimens in this investigation, equation (27) can be rewritten as

$$F_{1/2}(^*) = \frac{1.59 \times 10^3}{\mathcal{Q}_{123} \times T^{3/2}} \qquad (28)$$

The reduced Fermi level η^* can be evaluated from equation (28) if the temperature and the Hall coefficient are known.

In Figure 18, $\log \mathcal{Q}_{123}$ and the reduced Fermi level η^* are plotted as functions of the radiation dosage. The effect of irradiation is to decrease the Fermi level. From this it can be concluded that (1) the effect of proton irradiation is to introduce charged imperfections, in the compound Bi_2Te_3, (2) the majority of the charged imperfections are donors,
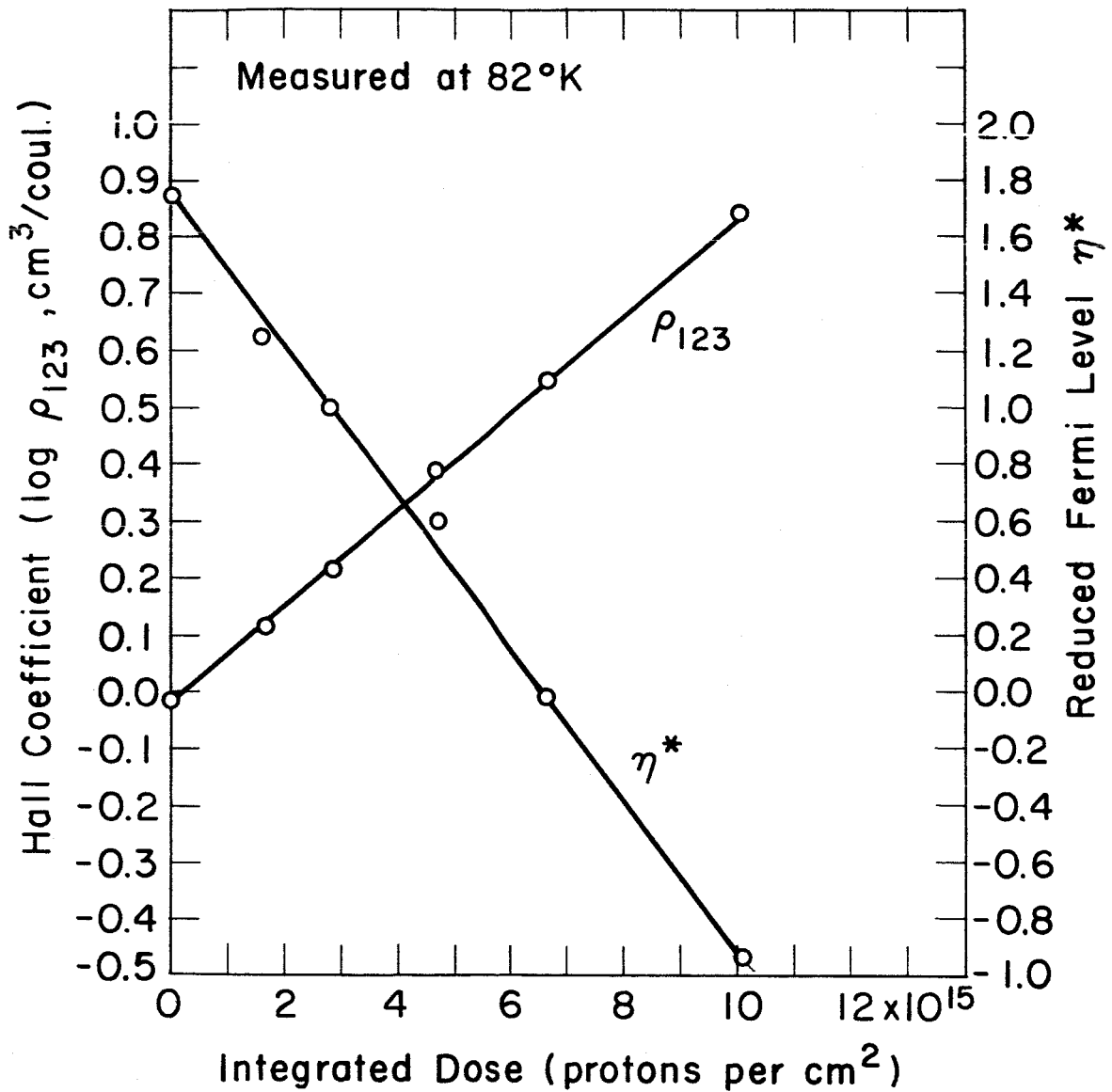
Figure 18. Hall coefficient and reduced Fermi level
as functions of integrated radiation dose.

and (3) the Hall coefficient is exponentially related to the irradiation dosage by the relation

$$\rho_{123} = (\rho_{123})_{\phi = 0} \; \exp (A \phi) \tag{29}$$

where A is equal to 1.96×10^{-16}, and ϕ is the integrated dose. Similarly an equation relating the reduced Fermi level and the integrated dose is given by

$$\eta^* = 1.75 - 2.67 \times 10^{-16} \phi \tag{30}$$

Equations (29) and (30) are equivalent in the sense that the Fermi Dirac integral of order 1/2, for the value of η^* involved here, is approximately proportional to $\exp \eta^*$.

1.2 Resistivity

The effect of proton irradiation is to increase the resistivity of the compound Bi_2Te_3. Such an increase is expected because irradiation is likely to introduce additional scattering mechanisms. The point defects introduced by the irradiation are ionized on neutral scattering centers. Both types of scattering centers increase the resistivity, but the temperature dependence of the resistivity is different in the two cases. The component of the resistivity due to neutral imperfections has been shown to be independent of temperature,[36] whereas the contribution to the resistivity made by ionized point imperfections changes with temperature.[37,38]

Since the temperature dependence of the resistivity varies with the irradiation dose (Figure 7) ionized scattering centers presumably are the dominant scattering centers. The conclusion can be verified by calculating the resistivity of the specimen as a function of temperature, as will be done in the next section, and comparing the calculated values with the experimental values.

1.2.1 Calculation of Electrical Resistivity - The reciprocal of the resistivity defined as the conductivity is given for a semiconductor of arbitrary degeneracy in which lattice scattering and ionized imperfection scattering are present by the expression

$$\sigma = \frac{\sigma_L}{\log(1 + \exp \eta*)} \int_0^\infty \frac{n^3 \exp (\eta - \eta*) \, d\eta}{(\eta^2 + \alpha) \left[\exp (\eta - \eta*) + 1 \right]^2} \tag{31}$$

where σ is the resultant conductivity if both lattice scattering and ionized imperfection scattering are present, σ_L is the conductivity which would result if only lattice scattering were present, $\eta*$ is the reduced Fermi level, and α is given by

$$\alpha = \frac{3 \, F_2(\eta*)}{\log (1 + \exp \eta*)} \frac{\sigma_L}{\sigma_i} \tag{32}$$

In this equation $F_2(\eta*)$ is the Fermi Dirac integral of order 2, and σ_i is the conductivity which would result if only ionized imperfections

were present.

The resistivity of the unirradiated specimen as a function of temperature was experimentally determined to be

$$\rho_{11} = 5.19 \times 10^{-8} \, T^{1.98} \tag{19}$$

in the temperature interval of 175 to 280°K. Assuming that this resistivity is due to lattice scattering, then the change in the value of the resistivity, due to lattice scattering after irradiation to an integrated dose ϕ, is given by

$$(\rho_{11})_L = 5.19 \times 10^{-8} \, T^{1.98} \; \frac{\log \, (1 + \exp \eta \ast)\phi = 0}{\log \, (1 + \exp \eta \ast)\phi} \tag{33}$$

The results[38] of ionized imperfection scattering can be combined with the information on the band structure[8] to give ρ_i, which can be written as

$$(\rho_{11})_i = \frac{\pi^3 \, e^2 \, h^3}{2(1 + u)\alpha_{11} m \ast K^2} \left(\frac{m}{m \ast} \right) \frac{N_i}{T^3} \frac{f(x)}{F_2(\eta \ast)} \tag{34}$$

In this equation, K is the dielectric constant, $m \ast$ is the effective mass, N_i is the number of ionized scattering centers per cm^3, and $f(x)$ is given by

$$f(x) = \log(1 + x) - \frac{x}{1 + x} \tag{35}$$

and

$$x = \frac{\bar{\eta}(kT)^{1/2} Kh}{e^2 (2m^*)^{1/2} f'_{1/2}(\eta^*)} \tag{36}$$

where $f'_{1/2}(\eta^*)$ is the derivative of the half-order Fermi-Dirac integral, and $\bar{\eta}$ is found from the equation

$$\frac{\bar{\eta}^2 + 3\alpha}{\bar{\eta}^3 + \alpha\bar{\eta}} = \tanh\left(\frac{\bar{\eta} - \eta^*}{2}\right) \tag{37}$$

The solution to equation (37) has been tabulated.[38] The Fermi-Dirac integrals of various orders required in these calculations have also been tabulated.[39] Since the values of α_{11}, α_{22}, m^* and the dielectric constant K are not known for the specimens, the resistivity given by equation (36) cannot be calculated. However, if it is assumed that the resistivity of the unirradiated specimen is due to contributions from lattice scattering and ionized imperfection scattering, then the constants in equation (34) can be evaluated by fitting the experimental values of resistivity at $82°K$ to the calculated values and assuming the dielectric constant to be 85; $(\rho_{11})_i$ can be written as

$$(\rho_{11})_i = \frac{N_i f(x)}{c\, T^3 F_2(\eta^*)} \tag{38}$$

where $(\frac{N_i}{c}) = 2.209 \times 10^5$. Using this form of the equation, the value of $(\frac{N_i}{c})$ can be obtained as a function of the radiation dosage. On the basis of these assumptions, σ was calculated from (31) as a function of temperature after successive irradiation doses. These values are shown by solid lines in Figure 19. The agreement between the experimental and calculated values is good. From this it can be concluded that apart from lattice scattering, the major scattering mechanism is ionized imperfection scattering.

In Figure 17, the band structure parameters were observed to change after an integrated dose of 10.1×10^{15} protons per cm^2, so that the value of the ratio $\frac{N_i}{c}$ changes not only due to a change in N_i, but also due to a change in c. The fractional change in the number of defects given in Figure 19 after irradiation to a dose of 10.1×10^{15} protons per cm^2 is, therefore, a fictitious number. In calculating the change in the resistivity the density of carriers was assumed to be constant over the entire temperature range for the specimens irradiated to an integrated dose less than 10.1×10^{15} protons per cm^2. After irradiation to this dose the actual value of the Hall coefficient was used to determine the change in the density of carriers with temperature. This was necessary because after the last irradiation dose the specimen started to show intrinsic behavior at low temperatures.
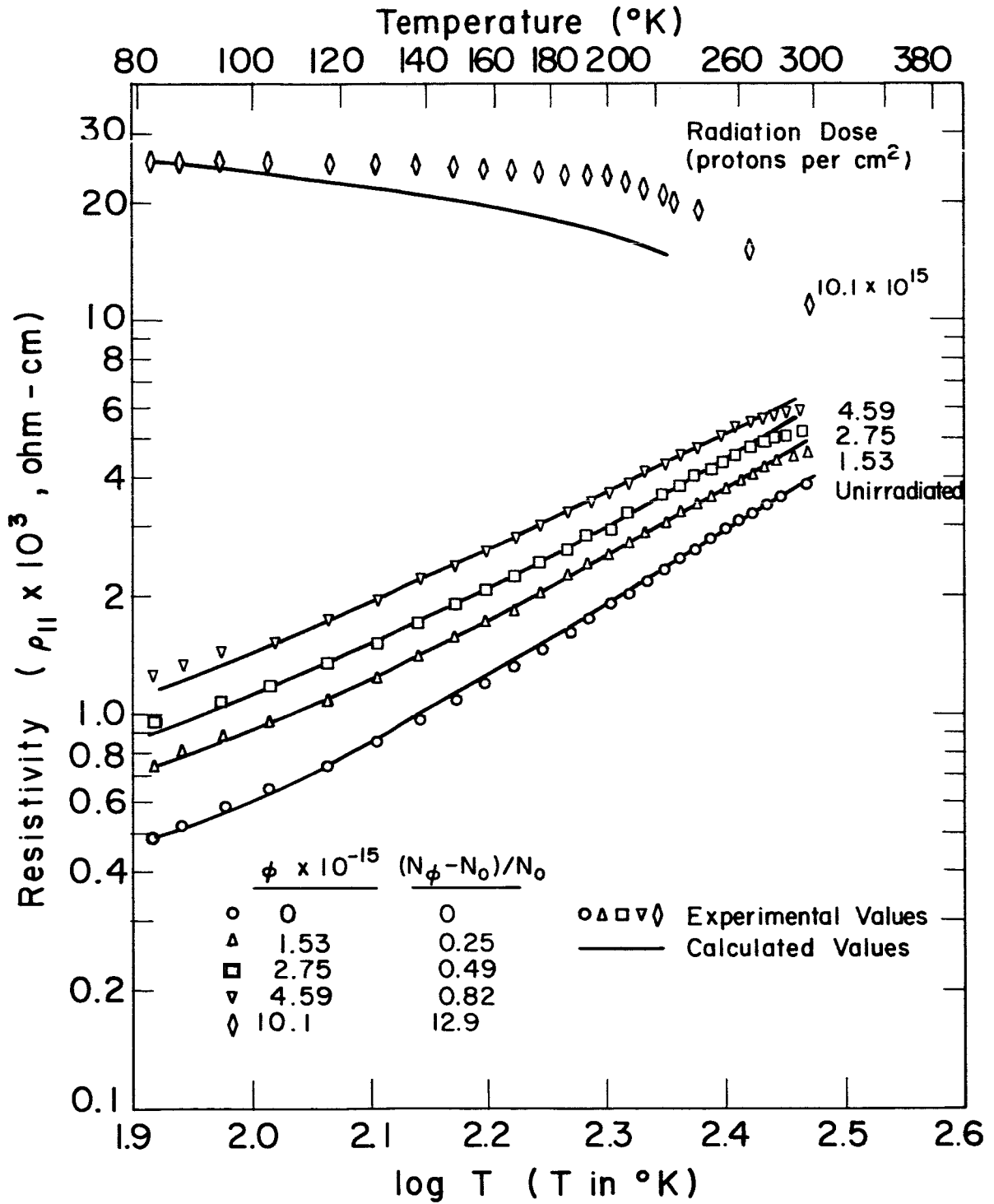
Figure 19 Experimental and calculated values of resistivity as functions of temperature after successive irradiations.

1.3 Rate of Defect Production

1.3.1 **Experimental Values** - The initial rate of defect production

with irradiation can be calculated from the experimental data by two methods:

(1) the change in the Hall coefficient by irradiation and (2) the change

in the value of the number of charged defects calculated from the change

in resistivity by irradiation. This number includes both the donors and

acceptors introduced by irradiation and should therefore be a better

approximation than the number calculated from the change in the Hall

coefficient. However, for the case where the number of acceptors and

donors may not be comparable, the change in the number of defects calculated

from the Hall coefficient data are likely to be more accurate because of

the assumptions involved in calculating the change in the number of

defects from the resistivity data. The change in the value of the Hall

coefficient with irradiation gives

$$\left(-\frac{dn}{d\phi}\right)_{\phi = 0} = 588 \tag{39}$$

where $\left(\frac{dn}{d\phi}\right)_{\phi = 0}$ may be called the rate of donor introduction into the

specimen by irradiation. The change in the value of the resistivity gives

$$\frac{dN}{d\phi} = 573 \tag{40}$$

This value is the average value of the number of defects introduced per proton. The values determined from the experimental data by the two methods can be compared with the values estimated from theory.

1.3.2 Values Estimated from Theory

In order to estimate the rate of defect production in the compound Bi_2Te_3, only the displacement and replacement mechanism of damage production will be considered. The number of primary knock-ons per unit length per proton is given by the equation[1]

$$\left(\frac{dp}{d\phi}\right) = N_o \, \sigma_d \tag{41}$$

where p is the number of primary knock-ons, ϕ is the radiation dosage, N_o is the number of atoms per unit volume, and σ_d is the displacement cross section. The number of primary knock-ons per unit length per proton calculated according to equation (41) is given in Table I. The two sets of values correspond to the two sets of values of the displacement energies E_d assumed. In the first set in which E_d is assumed to be equal to 7.5, 15, and 15 ev for atoms of $Te^{(1)}$, $Te^{(2)}$, and Bi, respectively, the displacement cross sections were calculated in Section IV, 2.2.2, and is given in equations (5), (6), and (7). In the second set E_d is assumed to be equal to 12.5, 25 and 25 ev for atoms of $Te^{(1)}$, $Te^{(2)}$ and Bi respectively.

Table I

RATE OF DAMAGE INTRODUCTION INTO Bi_2Te_3 WITH

7.5 Mev PROTONS

	Atom	Ed(ev)	p	Ed(ev)	p
Calculated number of primary	$Te^{(1)}$	7.5	290	12.5	173
knock-ons per cm^3 for two	$Te^{(2)}$	15	70	25	43
sets of displacement energies	Bi	15	<u>230</u>	25	<u>134</u>
			590		350

Total number of displacement collisions per cm^3 for two sets of displacement energies	3,250	2,700

Total number of displacement plus replacement collisions per cm^3 for two sets of displacement energies	18,600	15,400

Experimental values of the number
of defects per cm^3

Hall coefficient:	588
Electrical resistivity:	573

The number of defects that are introduced by the displacement cascade which follows each primary knock-on is difficult to estimate because of the presence of two types of atoms and their different displacement energies. A rough estimate can be made by replacing the actual compound by a hypothetical element, which has an atomic weight equal to the weighted average value of the compound Bi_2Te_3, and a displacement energy equal to the weighted average displacement energy of the compound Bi_2Te_3. The average number of displacement events $\bar{\nu}$ is given by[1,40]

$$\bar{\nu} = 0.12 + 0.56 \log E_{p(max)}/E_d \tag{42}$$

The total number of displacement events N is given by

$$\left(\frac{dN}{d\phi} \right) = \bar{\nu} N_o \sigma_d \tag{43}$$

The value of $\bar{\nu}$ has been calculated for two weighted displacement energies corresponding to the two sets of displacement energies assumed.

The ratio of the number of replacement to displacement events that occur following a primary knock-on is given by[41,42]

$$\frac{\bar{\nu}_r}{\bar{\nu}_d} = 1 + 1.614 \log \frac{E_d}{E_r} \tag{44}$$

where $\bar{\nu}_r$ is the average number of replacement collisions, and E_r is

the replacement energy. For E_d/E_r equal to ten[41] the ratio of replacement to displacement collisions is equal to 4.7. The total number of defects introduced by both displacement and replacement collisions is tabulated in Table I, the experimental values are also shown.

1.3.3 Comparison of Experimental and Theoretically Calculated Values of the Number of Defects -

In Table I it can be seen that the experimentally determined values are an order of magnitude smaller than the calculated values. This difference between the two values may be partly due to the approximation used in determining the number of replacement collisions because the assumed ratio of E_d/E_r equal to ten is probably too high for the compound Bi_2Te_3. The calculations for the number of displacement collisions does not take into account the effect of thermal and displacement spikes. Koehler and Seitz[43] have proposed that some of the defects anneal out during the time a thermal spike exists. Brinkman[44] has suggested that the main reason for the difference between the experimental and calculated values of the number of defects in materials irradiated with heavy particles is in the collapse of interstitial-vacancy pairs in a cluster which reaches a critical size due to a displacement spike.

Another reason for the difference between the experimental and calculated values is likely to be the annealing out of defects due to thermal activation, particularly interstitials lying between two $Te^{(1)}$ layers. Since the displacement energy of an atom is the $Te^{(1)}$ layer is half that of an atom in the other two types of layers, a greater number

of primary knock-ons occurs with these atoms. This can be seen in Table I. A large number of vacant sites on $Te^{(1)}$ layers must be therefore present. If the interstitial defects between $Te^{(1)} - Te^{(1)}$ layers can move because of thermal motion, a large number of vacancies will be annihilated. The tellurium atoms that are displaced from the $Te^{(1)}$ layers either occupy interstitial sites or replace bismuth and tellurium atoms. When the tellurium atoms occupy interstitial sites or replace bismuth atoms they act as donors.[12,13]

2. Transmission Electron Microscopy

The defect configurations in the irradiated specimens for electrical measurements are expected to be different from those in the specimens for examination by transmission electron microscopy because of the higher flux and larger integrated doses used for the specimens for electron microscopy. The difference in radiation dose was necessary because the point defect clusters after an integrated dose of 10^{16} protons per cm^2 were not expected to be sufficiently large and sufficiently numerous for examination by transmission electron microscopy. The higher flux introduces a large number of defects per unit time, and in comparison to the specimens irradiated at lower level of flux raises the temperature of the specimens during irradiation so that the ease of migration of the defects is increased. As a result point defect clusters rather than isolated point defects are expected to be present in the specimens.

If, however, the temperature of the specimens rises too high, the defects anneal out faster than they are formed. The migration of point defects also affects the dislocation configuration. Because of excess vacancies and interstitials the edge dislocations can climb non-conservatively, so that this supplies a mechanism for the rearrangement of dislocations.

2.1 Point Defects

During observation in the electron microscope clusters of point defects annealed out (Figures 12 and 13). This was attributed to heating of the specimen by the electron beam of the microscope. On heating specimens of the compound Bi_2Te_3 after exposure to γ-radiation at room temperature, Smith[19] found that some of the defects annealed out at $50^{\circ}C$. He attributed this to the dissociation of interstitial clusters and the migration of interstitials. It is possible that the clusters of defects observed in the electron microscope may be similar to those reported by Smith.[19]

The shape of defect clusters is affected by the bonding scheme. Because of the directional nature of covalent bonding, the smaller clusters in the compound Bi_2Te_3 may be expected to have shapes other than spherical so that the alignment of the major axis of some of the defect clusters in the $\langle 10\bar{1}0 \rangle$ and $\langle 11\bar{2}0 \rangle$ directions is probably due to this effect. With increasing size of the cluster, a vacancy loop lying on three of the six $\{20\bar{2}9\}$ planes with a major axis along the $\langle 11\bar{2}0 \rangle$ directions would be energetically more favorable

than a row of clusters aligned along the $\langle 10\bar{1}0 \rangle$ directions. In such a vacancy loop the largest number of bismuth-tellurium bonds broken lie within the plane of the loop and therefore a minimum amount of disruption of the structure results. Further, by nucleating a Shockley partial dislocation on the periphery of such a loop, the broken bonds may combine with bonds across the loop plane. Only three out of the six planes are chosen because the true structure of the compound Bi_2Te_3 is rhombohedral and not hexagonal.

The agglomeration of loops shown in the area marked X in Figure 14 is probably due to the movement of loops and their interaction with each other. Barnes[45] has suggested that this might be the explanation of some of the observations in irradiated graphite and copper. The clusters marked I in Figure 14 are not interstitial dislocation loops but are precipitates coherent with the lattice. This is because a dislocation loop lying on the basal plane with a Burgers vector parallel to the c-axis does not show diffraction contrast when the electron beam is parallel to the c-axis, the interstitial clusters shown in Figure 14 must therefore have a component of the Burgers vector in the plane of the foil. Since the contrast effects shown by the interstitial clusters are symmetrical about the c-axis, it follows that the clusters are not prismatic dislocation loops. The interstitial atoms present in clusters must therefore modify the bonding scheme locally so as to form precipitates which are coherent with the lattice.

The mechanism of formation of the hexagonal areas is not understood. One possible mechanism may be that the specimen was heated to a high temperature by the proton beam and in combination with the defects introduced by the protons initiated local evaporation of material from the surface of the specimen. Further evaporation from the edge created by the initial evaporation was easier so that areas with hexagonal shapes were formed. In order to confirm this mechanism the specimens were heated in the electron microscope by increasing the beam current. The hexagonal areas grew in size. No nucleation of areas similar to those in irradiated specimens was observed, indicating that a high temperature and vacuum was not sufficient to cause evaporation of the specimen locally but that defects were also required. Some of the hexagonal areas were observed to change to triangular areas, probably because the structure of the compound is rhombohedral and therefore under slow rate of removal material from the surface of the specimen, the triangular shape is energetically more favorable.

2.2 Line Defects

In the presence of point defects, edge dislocations can move non-conservatively by climb. Since a large number of point defects are introduced by irradiation the appearance of broken segments of edge dislocation lines can be taken as evidence that in these areas edge dislocations climbed out to the surface of the foil. The temperature rise in the specimens introduced stresses, particularly since the cooling

rate across the specimen was non-uniform.   As a result dislocation

movement occurred during irradiation.   The motion of the dislocations

was hindered by the presence of defect clusters so that these lines

were pinned and gave rise to the jagged appearance observed in

Figures 14 and 16.

VII. SUMMARY AND CONCLUSIONS

In this investigation single crystals of p-type Bi_2Te_3 were irradiated with protons of 7.5 Mev energy. The changes in the Hall coefficient, resistivity, and magneto-resistance of the specimen was measured after successive irradiations. Crystalline imperfections introduced by irradiation were examined in foils by transmission electron microscopy.

1. Electrical Measurements

1.1 Hall Coefficient

The value of the Hall coefficient of the compound Bi_2Te_3 increased with increasing radiation dosage. After an integrated dose of 1.2×10^{16} protons per cm^2, the specimen was converted from p-type to n-type. In the range of integrated doses in which the specimen was p-type, the Hall coefficient φ_{123} was exponentially related to the integrated dose by the equation

$$\varphi_{123} = (\varphi_{123})_{\phi = 0} \exp 1.96 \times 10^{-16} \phi \qquad (29)$$

where ϕ is the integrated dose. The net effect of irradiation was to introduce donors, which were fully ionized at $82^{\circ}K$. The value of the Fermi level decreased with increasing radiation dosage.

1.2 Electrical Resistivity

The resistivity of the specimen increased on irradiation. The

exponent of the temperature dependence of the resistivity decreased, and became negative, after a dose of 1.2 x 10^{16} protons per cm^2. The increase in resistivity with irradiation was due to a reduction of the number of charge carriers and to increased scattering of the charge carriers with increasing concentrations of ionized imperfections. Based on the assumption that the two major mechanisms of charge carrier scattering were ionized imperfection and lattice scattering, satisfactory agreement between the calculated and experimental values was obtained. This confirmed that the predominant effect of irradiation was to introduce ionized imperfections.

The number of defects calculated from the Hall coefficient and resistivity data was observed to be more than an order of magnitude smaller than values calculated from radiation damage theories. The difference in the two values is interpreted as evidence of annealing out of defects by the movement of interstitials between the two layers consisting of atoms of Te[1] type.

1.3 Coefficient of Magneto-resistance

The coefficient of magneto-resistance measured at 82°K decreased with increasing irradiation and appeared to reach a saturation value after a dose of 1.0 x 10^{16} protons per cm^2. The ratio of the band structure parameters calculated from the Hall coefficient, resistivity and magneto-resistance were observed to change rapidly after integrated doses of 1.0 x 10^{16} protons per cm^2.

2. Transmission Electron Microscopy

2.1 Point Defects

After irradiation to an integrated dose of 5.5×10^{18} protons per cm^2 at a flux of 1.8×10^{13} protons per cm^2-sec, point defect clusters ranging in size from 50 to 250 A.U. were observed. These clusters were observed to anneal out rapidly during observation in the electron microscope. Some of the clusters were observed to be aligned along the $\langle 10\bar{1}0 \rangle$ and $\langle 11\bar{2}0 \rangle$ directions.

After irradiation with an integrated dose of 5.5×10^{18} protons per cm^2 at a flux of 3.0×10^{13} protons per cm^2, clusters of interstitial atoms and vacancies were observed. The interstitial clusters were present in the form of coherent precipitates, presumably due to a rearrangement of the bonds locally.

Pits with hexagonal cross-sections parallel to $\langle 11\bar{2}0 \rangle$ direction were observed in some parts of the specimen. During examination in the electron microscope at high beam currents, these pits were observed to grow, and some of them changed shapes from hexagons to triangles. The pits are attributed to evaporation of the material from the surfaces at high temperatures in the presence of defects created by the irradiation.

2.2 Line Defects

The effect of irradiation was to cause dislocation climb, so that segments of a dislocation line were found to intersect the surface of the

specimen.   In addition, dislocation lines acquired a jagged shape due
to pinning down of the lines by defect clusters introduced by irradiation.

VIII. SUGGESTIONS FOR FURTHER WORK

1. The annealing behavior of specimens irradiated with protons should be investigated. From the changes in the electrical properties and the values of the activation energies the defects introduced by the irradiation can be identified more clearly than in the present investigation.

2. An examination of foils of the compound Bi_2Te_3 by transmission electron microscopy after irradiation with protons should be conducted more systematically with respect to changes in the integrated dose and flux. This examination should be extended to the compound Sb_2Te_3, which has the same structure and similar physical properties as Bi_2Te_3, but different arrangement of defects in unirradiated specimens.

3. Thin specimens of elemental semiconductors and metals should be irradiated at and below the temperature of liquid helium with electrons of sufficient energy to cause single displacement collisions. The displacement energy as a function of the crystal orientation and temperature of irradiation should be investigated. The annealing behavior of such specimens and specimens irradiated with electrons of higher energies should be examined.

4. Fission fragment damage in single crystals with selected orientations should be investigated by transmission electron microscopy. The damage in the wake of a fission fragment is sufficiently extensive that diffraction contrast mechanisms can be utilized to provide information on the nature of damage due to this cause.

APPENDIX

Range of 7.5 Mev Protons in Bi_2Te_3

The thickness of the specimen used in Hall coefficient and resistivity measurements is limited by the range of the incident particle in the specimen. An estimate of the range of the incident particle is therefore necessary in order to use a thickness such that no particle is retained in the foil. Since the displacement cross section of the atoms of the absorbing medium varies with the velocity of the incident particle, a knowledge of the velocity of the particle at any point in the foil is therefore also of interest.

The principal mechanism[30,45] by which heavy charged particles can lose energy in traversing a foil is by ionization and excitation of the absorbing atoms. For a particle of any spin having a rest mass M ($\gg$ m_o), charge z e, and velocity V (= βc), the energy transferred to the foil as excitation and ionization on traversing a path dr of the foil containing N_o atoms/cm^3, each of atomic number Z, is approximated[45] by

$$\frac{dE}{dr} = \frac{4\pi e^4 z^2}{m_o V^2} \quad NZ \left[\ln \frac{2m_o V^2}{I} - \ln (1 - \beta^2) - \beta^2 \right] \tag{1}$$

where e is the electronic charge, m_o is the rest mass of the electron, and I is the geometric mean ionization and excitation potential, and is set equal to kZ, where k varies between 10 and 15 ev.

Equation (1) can be integrated and yields the following expression

$$R_2 - R_1 = \frac{M}{Z^2} \frac{1}{32 \pi e^4 m_o} \frac{I^2}{NZ} (\bar{Y}_2 - \bar{Y}_1) \tag{2}$$

where $Y = Ei (\log \frac{2m_o v^2}{I})^2$ and is an exponental integral, which has been tabulated.[46]

For the compound Bi_2Te_3 and an incident proton beam of 7.5 Mev energy, the range-energy expression is as follows:

$$R_2 - R_1 = \frac{5M}{Z^2} \frac{1}{32 \pi e^4 m_o} \left\{ \left[\frac{I^2}{3N_o Z} (Y_2 - Y_1) \right]_{Te} + \left[\frac{I^2}{2N_o Z} (Y_2 - Y_1) \right]_{Bi} \right\} \tag{3}$$

where N_o is the number of atoms of bismuth and tellurium per cm^3 of the foil. For the two cases $k = 15$ e.v., and $k = 10$ e.v., Figure (A-1) shows the energy-range relationship, based on equation (3).

The maximum range for which an incident 7.5 Mev proton has dissipated all its energy as excitation and ionization can also be estimated[45] approximately by the Bragg-Kleeman rule, which can be stated as follows:

$$\frac{R_1}{R_o} = \frac{\rho_o}{\rho_1} \left(\frac{A_1}{A_o} \right)^{1/2} \tag{4}$$

where R_1, ρ_1, A_1 are the range, density and atomic weight, respectively
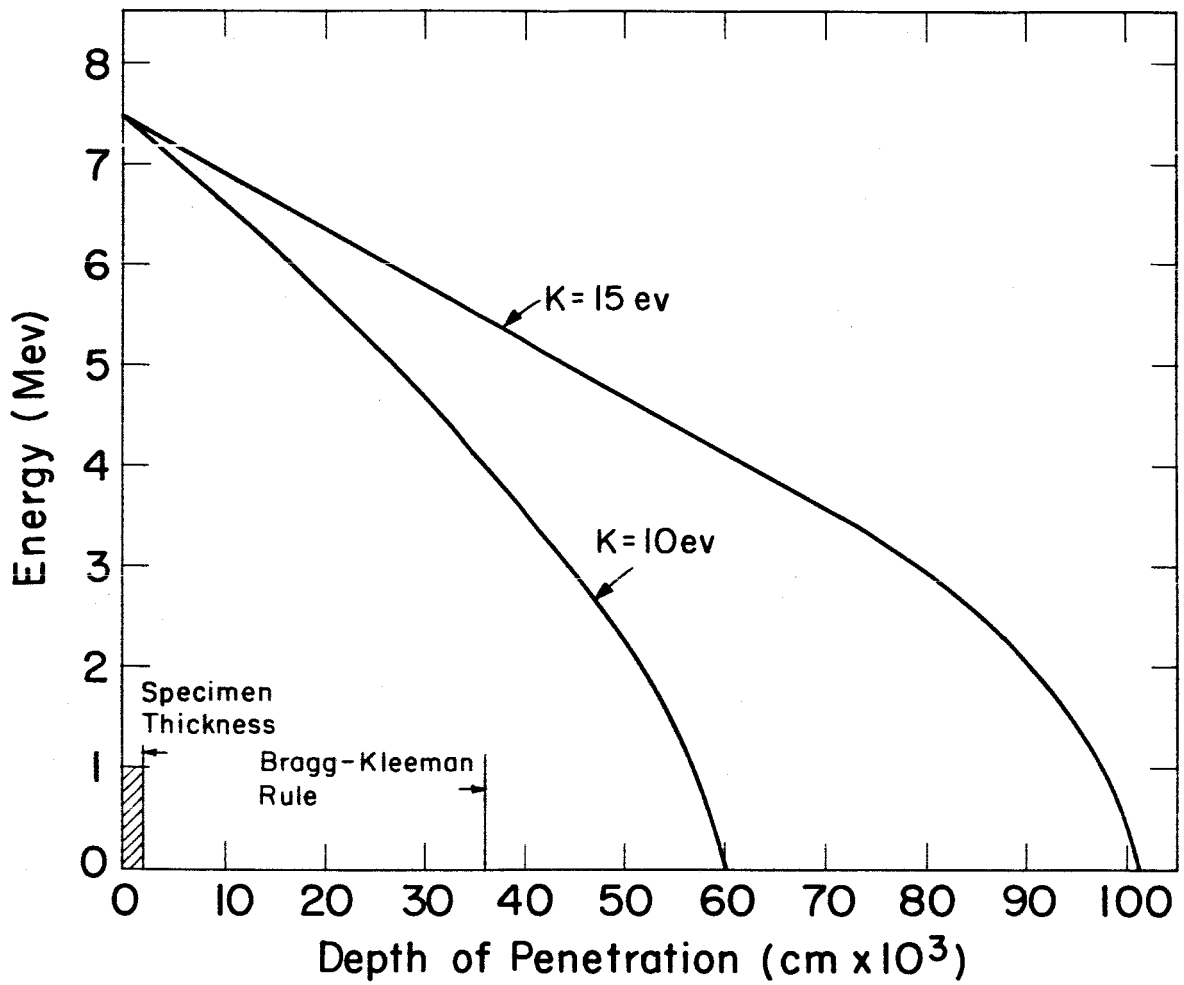
Figure A-I   Energy of the proton as a function of the depth of penetration.

of the incident particle in the absorbing material and R_o, ρ_o, A_o are the range, density and atomic weight, respectively, of the reference material, in which the range of the incident particle is known. For a compound $\sqrt{A} = n_1 \sqrt{A_1} + n_2 \sqrt{A_2}$, where n_1, n_2 are the atomic fractions of the elements whose atomic weights are A_1, A_2. If the reference material is air, then the Bragg-Kleeman rule for 7.5 Mev protons gives a range as 0.36 mm. for the compound Bi_2Te_3. This value corresponds more closely to the case of $k = 10$, in which this maximum range is about 0.60 mm, rather than the case of $k = 15$ in which it is about 1.01 mm.

REFERENCES

1.   Billington, D.S. and Crawford, J.H. - "Radiation Damage in Solids",
     Princeton University Press, Princeton (1961).

2.   Heikes, R.R. and Ure, Jr., R.W. - "Thermoelectricity, Science and
     Engineering", Interscience, New York (1961).

3.   van Allen, J.A. - "The Geomagnetically Trapped Corpuscular Radiation"
     J. Geophys. Res., $\underline{64}$, 1683 (1959).

4.   Lange, P.W. - "Ein Vergleich Zwischen Bi_2Te_3 und Bi_2Te_2S", Naturwiss.,
     $\underline{27}$, 133 (1939).

5.   Francombe, M.H. - "Structure-Cell and Expansion Coefficients of
     Bismuth Telluride", British J. Appl. Phys., $\underline{9}$, 415 (1958).

6.   Drabble, J.R. and Goodman, G.H. - "Chemical Bonding in Bismuth
     Telluride", J. Phys. Chem. of Solids, $\underline{5}$, 142 (1958).

7.   Delavignette, P. and Amelinckx, S. - "Dislocation Nets in Bismuth and
     Antimony Tellurides", Phil. Mag., $\underline{5}$, 729 (1960).

8.   Drabble, J.R. - "Galvanomagnetic Effects in P-Type Bismuth-Telluride",
     Proc. Phys. Soc. (London), $\underline{72}$, 380 (1958).

9.   Black, J., Conwell, E.M., Seigle, L., and Spencer, C.W. - "Electrical
     and Optical Properties of Some M_2^{V-B} N_3^{VI-B} Semiconductors", J. Phys.
     Chem. Solids, $\underline{2}$, 240 (1957).

10. Satterthwaite, C.B. and Ure, Jr., R.W. - "Electrical and Thermal
     Properties of Bi_2Te_3", Phys. Rev., $\underline{108}$, 1164 (1957).

11. Bergmann, G. - "Untersuchungen uber Fehlordnungserscheinungen an
     Bi_2Te_3", Angew. Chem., $\underline{76}$, 58 (1964).

12. Harman, J.C., Miller, S.E., and Goering, H.L. - "Preparation and
     Electrical Properties of Bi_2Te_3", Bull. Am. Phys. Soc. $\underline{30}$, 35 (1955).

13. Miller, G.L. and Li, Che-Yu. - "Evidence for the Existence of Anti-
     structure Defects in Bismuth Telluride by Density Measurements",
     J. Phys. Chem. Solids, $\underline{26}$, 173 (1965).

14. Birkholz, V.U. - "Untersuchung der Intermetallischen Verbindung Bi_2Te_3
     sowie der Festen Losungen $Bi_{2-x}Sb_xTe_3$ und $Bi_2Te_{3-x}Se_x$ hindsichtlich
     ihren Eingung als Material für Halbleiter-Thermoelemente", Z. Natur-
     forsch., $\underline{13}$, 785 (1958).

15. Kokosh, G.V. and Sinani, S.S. - "Thermoelectric Properties of Alloys of the Pseudobinary System Sb_2Te_3-Bi_2Te_3", Fizika Tverdogo Tela, 2, 1118 (1960). English Translation: Soviet Physics - Solid State, 2, 1012 (1960).

16. George, W.E., Sharples, R., and Thompson, J.E. - "The Sintering of Bismuth Telluride", Proc. Phys. Soc. (London), 74, 768 (1959).

17. Schultz, J.H., McHugh, J.P., and Tiller, W.A. - "Effects of Heavy Deformation and Annealing on the Electrical Properties of Bi_2Te_3", J. Appl. Phys., 38, 2443 (1962).

18. Artman, R.A. and Goland, A.N. - "Effect of Υ Irradiation on Thermoelectric Power of Bismuth Telluride", Bull. Am. Phys. Soc., 5, 168 (1960).

19. Smith, M.J. - "$Co^{60}\Upsilon$ - Radiation-Induced Point Defects in Bi_2Te_3", J. Appl. Phys., 34, 2879 (1963).

20. Levy, R.A. - "Radiation Effects on Thermoelectric Power in Bi_2Te_3", Bull. Am. Phys. Soc., 5, 168 (1960).

21. Corelli, J.C., Frost, R.T., and White, F.A. - "Effect of Reactor Irradiation on Thermoelectric Properties of PbTe and Bi_2Te_3", Bull. Am. Phys. Soc., 5, 168 (1960).

22. Balicki, M., Corelli, J.C., and Frost, R.T. - "Metallurgy of Elemental and Compound Semiconductors", 12, Interscience Publishers, Inc., New York (1961).

23. Artman, R.W. - "Neutron Irradiation of Bismuth Telluride", Bull. Am. Phys. Soc., 1, 187 (1962).

24. Delavignette, P., and Amelinckx, S. - "Large Dislocation Loops in Antimony Telluride", Phil. Mag., 6, 601 (1961).

25. Bierly, J.N. - "Vacancy Loops in the Pseudo-Binary Alloy BiTe-SbTe", Proc. 5th Intern. Conf. on Electron Microscopy, Philadelphia, 1, J-14 (1962).

26. Bollmann, J. - "Radiation Damage in Graphite", J. Appl. Phys., 32, 869 (1961).

27. Williamson, G.K. and Baker, C. - "A Comparison of Vacancy and Interstitial Loops in Graphite", Phil. Mag., 6, 313 (1961).

28. Groves, G.W. - "Radiation Damage in MgO", Proc. 5th Intern. Conf. on Electron Microscopy, Philadelphia, 1, F-10 (1962).

29. Dennis, J.H. - "Anisotropy of Thermoelectric Power in Bismuth Telluride", Ph.D. Thesis, Massachusetts Institute of Technology, Cambridge, (1961).

30. Seitz, F. and Koehler, J.S. - "Displacement of Atoms during Irradiation", Solid State Physics, 2, 307 (1956), edited by F. Seitz and D. Turnbull, Academic Press, New York (1956).

31. Rappaport, P., and Loferski, J.J. - "Threshold for Electron Bombardment Induced Lattice Displacements in Si and Ge", Phys. Rev. 100, 1261 (1955).

32. Isenberg, K., Russell, B.R., and Greene, R.F. - "Improved Method for Measuring Hall Coefficients", Rev. Sci. Instrum., 19, 685 (1948).

33. Hirsch, P.B., Howie, A., and Whelan, M.J. "A Kinematical Theory of Diffraction Contrast of Electron Transmission Microscope Images of Dislocations and Defects", Phil. Trans. Roy. Soc., A 252, 499 (1960).

34. Bell, W., Maher, D.M. and Thomas, G. - "Vacancy Aggregates in Quenched Copper Single Crystals", Lattice Defects in Quenched Metals, edited by Cotterill, M.J., Doyama, M., Jackson, J.J., and Meshii, M., Academic Press, New York (1965).

35. Ashby, M.E., and Brown, L.M. - "Diffraction Contrast from Spherically Symmetrical Coherency Strains", Phil. Mag. 8, 1083 (1963).

36. Erginsoy, C. - "Neutral Impurity Scattering in Semiconductors", Phys. Rev., 79, 1013 (1950).

37. Debye, P.P. and Conwell, E. - "Electrical Properties of N-Type Germanium", Phys. Rev., 93, 693 (1954).

38. Mansfied, R. - "Impurity Scattering in Semiconductors", Proc. Phys. Soc. (London), B69, 76 (1956).

39. Blakemore, J.S. - "Semiconductor Stastics", 3 (1962), edited by Henisch, H.K., International Series of Monographs on Semiconductors, Pergamon Press, New York (1962).

40. Harrison, W.A. and Seitz, F. - "On the Theory of Radiation Damage", Phys. Rev., 98, 1530 (1955).

41. Kinchin, G.H. and Pease, R.S. - "The Mechanism of Irradiation Disordering of Alloys", J. Nuclear Energy, 1, 200 (1955).

42. Dienes, G.J. and Vineyard, G.H. - "Radiation Effects in Solids", Interscience, New York (1957).

43. Koehler, J.S. and Seitz, F. - "Nature of Irradiation Damage in Noble Metals", $\underline{31}$, 45 (1961).

44. Brinkman, J.A. - "Radiation Production and Radiation Annealing of Point Defects in Metals", Proc. Intern. Conf. on Crystal Lattice Defects, J. Phys. Soc., Japan, $\underline{18}$, Supplement III,(1963).

45. Barnes, R.S. - "The Migration of Large Clusters of Point Defects in Irradiated Metals", Proc. Intern. Conf. on Crystal Lattice Defects, J. Phys. Soc., Japan, $\underline{18}$, Supplement III (1963).

46. Evans, R.D. - "The Atomic Nucleus", McGraw-Hill Book Co., (1955).

47. Tables of Sine, Cosine and Exponential Integrals, Vol. 2, National Bureau of Standards, Washington, D.C. (1940).

BIOGRAPHICAL NOTE

The author was born on November 30, 1937 in Ludhiana, India. His primary and secondary schooling was completed in private schools. He joined the Indian Institute of Technology, Kharagpur in July 1957 and graduated with a B. Tech (Hons.) in Metallurgy in June 1961. He ranked first in his class and was a recipient of the Institute Scholarship from 1959 to 1961. In September 1961, he joined the Massachusetts Institute of Technology, Cambridge, as a graduate student and research assistant in the Department of Metallurgy. He obtained his S.M. degree in Metallurgy in June 1963.

The author is a student member of A.I.M.E., A.S.M. and the Indian Institute of Metals, and a member of the Society of Sigma XI.

The author was married on June 13, 1964 to the former Miss Karin Rømhild of Aarhus, Denmark. During the summer of 1964, he worked with the Research Establishment, Danish Atomic Energy Commission, Risø, Denmark.

The following two notes by the author have been accepted for publication:

Chaudhari, P.   -   "Frank-Read Sources in Ordered Alloys", Acta Metallurgica, in press.

Chaudhari, P. and Scattergood, R.O. - "Pile-Up Models for Yielding", Acta Metallurgica, accepted for publication.